A novel 3D bioprinted model of Alzheimer's disease using patient derived hiPSC derived neurons in a fibrin-based hydrogel bioink

by

Jonathan Walters-Shumka

A Thesis Submitted in Partial Fulfillment

of the Requirements for the Degree of

BACHELOR OF SCIENCE (HONOURS)

in the Faculty of Science, Department of Biology

University of Victoria

Supervisory Committee Members

Dr. Stephanie Willerth (Division of Medical Sciences)

Supervisor

Dr. Jürgen Ehlting (Department of Biology)

Supervisor

Dr. Katherine Elvira (Department of Chemistry)

External Examiner

Dr. Steve Perlman (Department of Biology)

Honours Advisor

Abstract

Alzheimer's Disease (AD) is an age-related neurodegenerative disease that does not yet have any disease modifying treatments. Because there is a high cost associated with the disease and because the prevalence of AD is increasing, the need for new drugs to treat AD is high. Many drugs have passed pre-clinical trials only to fail in clinical trials. Most of the pre-clinical trials have been conducted on 2D monolayer cell culture and animal models. The failure of these drugs in clinical trials indicates that these two kinds of models do not accurately model AD. A 3D bio printed hydrogel model of AD which uses familial AD (fAD) patient derived human induced pluripotent stem cells (hiPSCs) can provide a more accurate model. Here we describe the first steps in creating a novel 3D bio printed model of AD using hiPSCs derived from a patient with a fAD mutation on the APP gene and a healthy control hiPSCs line. We 3D printed ring-shaped constructs 8mm high and 1cm wide containing fAD and healthy patient derived hiPSC derived neural progenitor cells (NPC's). The 3D printed constructs were then differentiated for 45 days in a cortical neuron differentiation medium. We have shown that both the AD and healthy cell lines are able to produce neurite extensions and stain positive for the early neuronal cytoskeleton marker ß tubulin III in our bioink. This indicates that the cells have successfully differentiated into neurons within our bioink. We have also observed axonal boutons, and dendritic spines on both cell lines and an axonal swelling on an AD neuron which is associated with early AD pathology. These findings confirm past work that healthy and diseased patient derived hiPSC derived neurons can be differentiated in hydrogel scaffolds. This is however, the first time this has been done in 3D printed hydrogel scaffolds. This is also the first

time that dendritic spines and axonal swellings have been observed in a 3D hydrogel model of AD.

Table of Contents

List of Tables

List of Figures

Acknowledgements

I would like to thank the Dr. Haakon Nygaard lab for supplying us with our cell lines and culturing protocols which have made this project possible.

I would also like to thank everyone in the Willerth lab especially Kali, Nadia and specifically Ruchi for helping me with printing, making bioink and for helping me whenever I had questions. I would also like to thank everyone in the Willerth and Swayne labs for working so hard to accommodate everyone's schedules in shared labs spaces during the pandemic. Also, a special thank you to Juan Triviño Paredes for performing confocal microscopy for me during the pandemic.

Thank you to my honours advisor Dr. Steve Perlman for working so hard to keep us on track and for his guidance throughout the honours process.

And thank you to my co-supervisor Dr. Jürgen Ehlting for agreeing to be my co-supervisor and for all of his guidance with writing and the honours program.

Most of all I would like to thank Dr. Stephanie Willerth and Christopher Lee. I would like to thank them for giving me the opportunity to work on such an interesting project and for their guidance and encouragement throughout it. Working on this project for the last 2 years has been the best learning experience of my life.

Dedication

To my parents Jean and Gary and my sisters Annie and Kistina for their endless love and support. I would also especially like to thank my girlfriend Sam for supporting and encouraging me and for not getting too upset when I go to the lab at midnight.

Chapter 1: Introduction

1.1 Alzheimer's Disease:

Alzheimer's disease (AD) is a neurodegenerative disease that is the most common cause of dementia (Prince *et al.* 2016). AD results in the death of neurons primarily in the hippocampus and cortex of the brain, eventually leading to the death of the patient and the distinctive atrophied appearance of the brain (DeTure & Dickson, 2019). Dementia is defined as a decline in cognitive function that interferes with the normal functioning of the patient. (Chertkow, 2014). Diagnosis of AD includes first the diagnosis of dementia and then the diagnosis of probable AD because actual diagnosis of AD can only be confirmed with a post-mortem analysis of the patient's brain tissue (McKhann, 2011).

AD, a multifactorial disease, has many risk factors including a family history of AD, genetics, epigenetics, traumatic brain injury, low level of education, diet, immune system dysfunction, and vascular disease (Lindsay, 2002; Armstrong, 2010). AD prevalence increases with age, which is the largest risk factor of AD as approximately 3% of people age 65-74, 17% of people age 75-84, and 32% of people older than 84 have AD (Alzheimer's Association, 2019). Only 3 % of AD cases are found in people under the age of 65. The United Nations estimates that the proportion of people over the age of 65 will increase to 16% in 2050 from 9% in 2019. As the age of the population increases so will the incidence of AD. In 2015 it was estimated that 46.8 million people have AD worldwide and that by 2030 that number will increase to 74.7 million (Prince *et al.* 2016). The cost associated with AD is also significant. In 2015 this cost was estimated to be 818 billion USD. By 2030 this number is expected to reach 2 trillion USD.

1.2 Tau and Amyloid Beta

First discovered by Alois Alzheimer in 1906 Amyloid Plaques and Neurofibrillary tangles (NFTs) are now accepted as the two major pathological hallmarks of Alzheimer's disease (Hippius & Neundörfer, 2003). Amyloid plaques are caused by a buildup of Amyloid Beta (Aß) protein. Aß was first isolated in 1984 (Glenner, 2012). Aß protein is derived from the proteolytic processing of amyloid precursor protein (APP)(figure 1)(Chen *et al.* 2017). APP is a transmembrane protein and is a member of the APP protein family which includes APP, amyloid precursor-like protein 1 (APLP-1), and amyloid precursor like protein 2 (APLP-2) (Walsh *et al.* 2007). There are three isoforms of APP: APP695, APP751, and APP770 (Zhang *et al.* 2011). The Aß region of APP is typically 40 or 42 residues long (Kakuda *et al.* 2006). APP undergoes significant post translational processing and is found in high concentrations in neuronal cells. After processing and sorting in the endoplasmic reticulum and trans golgi network (TGN), APP is packaged in vesicles and sent to the cell membrane (Toh *et al.* 2017).

Non-amyloidogenic processing of APP primarily occurs in the outer plasma membrane of the cell after the vesicles from the TGN fuse with the membrane exposing the N-terminus of APP to the extracellular space (O'Brien & Wong, 2011)(figure 1). APP is cleaved extracellularly by the enzyme alpha secretase between the lysine 16 and leucine 17 residues within the Aß domain thereby preventing Aß production during non-amyloidogenic APP processing (Anderson *et al.,* 1991). The N terminus of APP, now called secreted APP-alpha (APPsα), is released into the extracellular space (Mockett *et al.,* 2017). The C-terminal fragment alpha (CTFα) is left within the membrane (Kojro & Fahrenholz, 2005). CTFα is then cleaved by gamma secretase at the end of the Aß region into the p3 region and the APP intracellular

fragment (AICD). The p3 region is then released into the extracellular space and AICD is released intracellularly.

Amyloidogenic APP processing occurs primarily within endosomes and in the TGN, though it can also occur on the endoplasmic reticulum and on the cell surface (Choy *et al., 2012*; Zhang & Song, 2013; Cook *et al.,*1997; Soriano *et al.*, 1999). First, APP is cleaved into secreted APP-beta (APPsß) and C-terminal fragment beta (CTFß) by the enzyme beta secretase (BACE-1)(figure 1). BACE-1 is a single pass transmembrane aspartyl protease that cleaves APP between positions 671 and 672 (Sinha *et al.* 1999; Vassar, 2003).

CTFß is then cleaved by gamma secretase into Aß in the place of the p3 fragment and into AICD. Variability in gamma secretase cleavage position accounts for Aß of different lengths (Holmes *et al.*, 2012). 40 or 42 residue long Aß is the most common length Aß produced (Qiu, 2015). Aß 42 forms amyloid plaques more readily and is more toxic than Aß 40. Aß monomers form Aß oligomers which then form amyloid plaques. There is evidence that amyloid oligomers cause many of the toxic effects associated with AD including activation of apoptotic pathways, oxidative stress, synapse loss and disruption of long-term potentiation (Sakono & Zako, 2010).

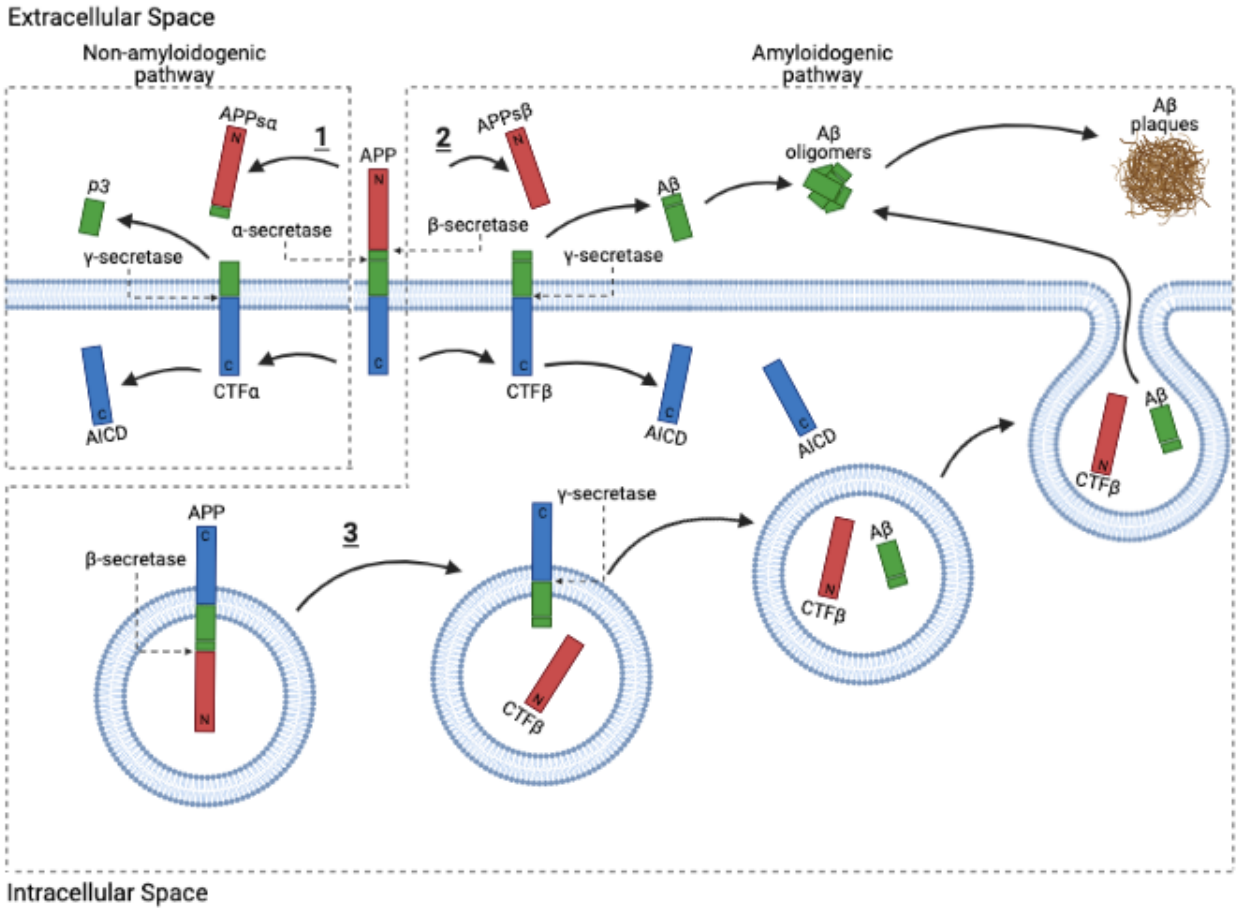

Figure 1: Processing of amyloid precursor protein

(1) Non-amyloidogenic APP pathway in the outer plasma membrane. (2) Amyloidogenic APP pathway. (3) Intracellular amyloidogenic APP processing.

The other hallmark of AD, neurofibrillary tangles, are caused by hyperphosphorylation of the protein tau (Grundke-Iqbal *et al.*, 1987). Tau is the predominant microtubule associated protein (MAP) in neuronal tissue (Weingarten *et al.*, 1975). It promotes the assembly of tubulin into microtubules and stabilizes their structure. There are six isoforms of tau due to the alternative splicing of the *TAU* gene on chromosome 17 (Neve *et al.,* 1986; Goedert *et al., 1989*). Multiple of these tau isoforms are hyperphosphorylated and incorporated into NFTs. Tau is a phosphoprotein and the level of phosphorylation of tau is regulated by different kinases and

phosphatases. Normally there are 2-3 moles of phosphate per mole of tau protein. Hyperphosphorylated tau has up to 3-4x more phosphorylation than normal tau (Köpke *et al.* 1993). Hyperphosphorylated tau also self-assembles into paired helical filaments (PHF)(figure 2)(Alonso *et al.* 2001). NFTs are aggregates of PHFs. There are 85 total phosphorylation sites on tau (Kimura *et al.,* 2018; Hanger *et al.,* 2007). 45 of these sites are on serines, 35 on threonines and 5 on tyrosine residues. Phosphorylation of each of these sites and combinations of these sites have different effects on the function of tau. Because of the large number of combinations of phosphorylation sites, not all of the effects of tau phosphorylation have been documented. However, some sites have been identified to be important in AD pathophysiology. For example, hyperphosphorylated tau has been shown to sequester MAP1, MAP2 and normal tau to form NFTs (Alonso *et al.* 1997). It has also been shown to promote the depolymerization of microtubules. Tau hyperphosphorylation occurs because tau kinases are overactive compared to tau phosphatases. The most prominent kinase involved in tau hyperphosphorylation is glycogen synthase kinase-3. Other significant kinases include cyclin-dependent kinase-5, and p38 MAP kinase. Hyperphosphorylated tau has a number of toxic effects including disruption of transport within the cell, as well as being a physical barrier in the form of NFTs (Götz *et al.,* 2013; Lin *et al.,* 2003; Ittner *et al.,* 2008). NFTs have been found to more accurately indicate the progression of AD than amyloid plaques though amyloid beta levels are still important in indicating the progression of the disease (Bierer *et al.,* 1995).

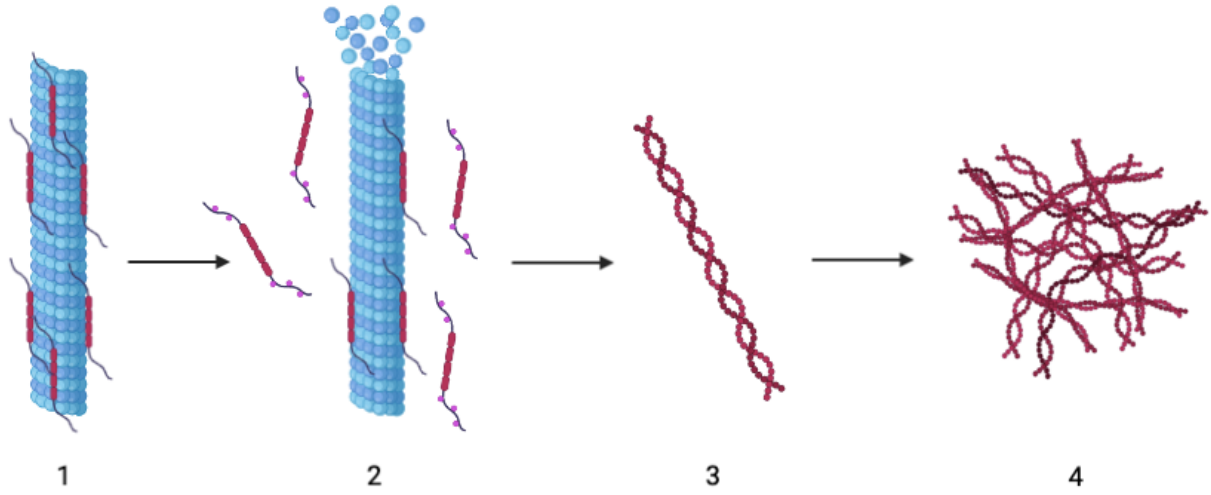

Figure 2: Pathway from normal tau protein to neurofibrillary tangles

(1) normal tau associating with and stabilizing a microtubule. (2) Hyperphosphorylated tau disassociating from the microtubule. The microtubule depolymerizes. (3) Paired helical filament forms from hyperphosphorylated tau. (4) Neurofibrillary tangle forms from aggregation of PHFs.

According to the amyloid cascade theory, which has been the predominant theory of AD since the 1990s, tau hyperphosphorylation and all other AD related effects are downstream effects of accumulation of Aß plaques. New evidence suggests that this may not be the case and that Aß likely plays a more indirect role than originally thought (Busche & Hyman, 2020; Barker, 2017). However, we still do not have a complete picture of the mechanisms behind the development of, and progression of AD.

1.3 Familial and Sporadic AD

AD comes in two forms: familial AD (fAD) and sporadic AD (sAD). fAD is monogenic and accounts for approximately 1% of AD cases (Piaceri *et al.,* 2013). fAD can be caused by mutations in the *APP* gene on chromosome 21, Presenilin 1 (*PSEN1*) gene on chromosome 14

and the Presellin 2 (*PSEN2*) gene on chromosome 1. fAD causing mutations in the *APP* gene have a variety of effects on the processing of APP most resulting in higher total Aß production and a higher Aß 42/40 ratio (Tcw, & Goate, 2017). Trisomy 21 (Downs syndrome) also causes an increase in Aß production and Aß plaque formation (Wisniewski *et al.,* 1985).

Presellins are subunits of the gamma secretase enzyme which catalyze the cleavage of CTFß and Aß. There are over 150 mutations of *PSEN1* causing fAD. It is also the cause of 70% of fAD cases (Medline Plus, 2020). Like *APP* mutations, *PSEN1* mutations also cause an increase in the total Aß and Aß 42/40 ratio (Shen & Kelleher, 2006). There are 11 *PSEN 2* mutations that cause fAD. These mutations only account for 5% of fAD cases. These mutations also increase the Aß 42/40 ratio (Walker *et al.,* 2005)

sAD is multifactorial and there have been many genes and risk factors associated with its development. The most important gene that modulates the risk of developing sAD is the *APOE* gene. *APOE* encodes for apolipoprotein E which is involved in the transport of lipids. There are 3 alleles of the *APOE* gene: e2, e3, and e4. The e3 allele is the most common and is found in roughly half of the population. The *APOE* e4 allele is the largest genetic risk factor for developing sAD (Liu *et al.,* 2013). Other risk factors include age, ethnicity, sex, traumatic brain injury, depression, cardiovascular disease and sleep disorders (Rabinovici, 2019). Protective factors include a high level of education, physical activity and social engagement.

1.4 AD Modeling Using Human Induced Pluripotent Stem Cells

Induced pluripotent stem cells (iPSCs) were first discovered in 2006 by Takahashi and Yamanaka. This was done through the transgenic addition of the four embryonic transcription factors, Oct3/4, Sox2, c-Myc, and Klf4 to a culture of adult mouse fibroblasts (Takahashi, & Yamanaka, 2006). The next year human induced pluripotent stem cells (hiPSCs) were derived from adult human fibroblasts using the same four factors (Takahashi *et al.,* 2007). hiPSCs are also typically derived from peripheral blood samples (Haase *et al.,* 2019). hiPSCs can then be differentiated into any somatic cell. This was a landmark discovery for the fields of stem cell research and disease modeling. hiPSCs offer a few key advantages over embryonic stem cells (ESC). One key advantage is that there are fewer ethical concerns associated with the use of hiPSCs over ESCs. Additionally, hiPSCs can be derived directly from patients. Patient derived hiPSCs are useful because they share their genetics with the patient. hiPSCs derived from patients with diseases which are in part caused by a genetic mutation, such as fAD, will also have that mutation. In the case of AD, patient derived hiPSCs are most commonly differentiated into cortical neurons (Arber *et al.,* 2017). Cortical neurons from these patient derived hiPSC models have been shown to have an increased Aß 42/40 ratio and hyperphosphorylated tau. This is useful for drug discovery as these are the targets of many of the pharmaceuticals currently being tested. It is thought that if a drug were to be found to decrease the Aß 42/40 ratio and/or hyperphosphorylated tau in hiPSCs it may be successful at treating AD in humans.

Before being differentiated into cortical neurons hiPSCs must be differentiated into neural progenitor cells (NPC) in a process called neural induction. NPC's are an intermediate between stem cells and glial or neuronal cells found in the central nervous system (CNS) (Zheng

et al. 2018; Martínez-Cerdeño & Noctor, 2018). There are two common pathways for the production of NPC's. The first method of neural induction is by first producing embryoid bodies (EB) from hiPSCs and then differentiating into NPC's. EBs are iPSCs that spontaneously group together in a process called gastrulation while in suspension (Baker, 2008). EB formation however can be inconsistent. EBs can aggregate causing variability in size which can affect the differentiation of the hiPSCs. iPSCs can also be directly differentiated into NPC's in a 2D monolayer. 2D differentiation does not have the size heterogeneity issues associated with EB formation. 2D differentiation is also easier to perform, takes less time and is more efficient (Galiakberova & Dashinimaev, 2020).

Dual inhibition of mothers against decapentaplegic (SMAD) signaling has been found to be important for the neural induction of hiPSCs (Chambers *et al.* 2009.) The activin, bone morphogenic protein (BMP), and transforming growth factor-β pathway inhibitor SB431542, and the BMP pathway inhibitor LDN193189 used in combination have been found to induce neural induction of hiPSCs (Chambers *et al.* 2012; Chambers *et al.* 2009). During neural induction neural rosettes are formed. Neural rosettes are spontaneously forming radial groups of columnar neuroepithelial cells that are markers of proper neural induction (Wilson & Stice, 2006). They resemble a cross section of the neural tube, the precursor of the CNS in human embryos. The NPC's can then be differentiated into cortical neurons. It has been shown that in a 2D monolayer, cortical neurons have been successfully differentiated from human NPC's in cultures containing brain derived neurotrophic factor, glial derived neurotrophic factor, cyclic AMP and ascorbic acid (Haase *et al.,* 2019).

1.5 Challenges of Modeling AD

Treatment options for AD are limited. There are currently four approved drugs to treat AD. Rivastigmine, Galantamine, and Donepezil are acetylcholinesterase inhibitors and memantine is a NMDA receptor inhibitor (Alzheimer's Association, n.d.). These drugs help to alleviate some of the symptoms of AD such as confusion and behavioural changes and memory loss for some patients. None of these drugs cure or change the course of the disease. There have been many clinical trials of disease modifying treatments of AD mostly focusing on decreasing NFTs and Aß plaques. None of the drugs have been successful in clinical trials (Mangialasche *et al.*, 2010). A large number of preclinical trials have been conducted using 2D cell culture and animal models. The low success rate of clinical trials indicates that these preclinical models are not sufficient. This is likely due to the differing physiology and genetics of animal models and the inability of 2D cell culture to recapitulate the extracellular environment and interactions experienced by cells *in vivo* (Jensen, & Teng, 2020; Perlman, 2016). A 3D bioprinted model of AD may be a solution to this problem.

1.6 3D disease modeling

Modeling neurological diseases using 3D printing technology is advantageous as it is a more accurate and reproducible method of creating biologically relevant neural tissue. Compared to a 2D culture, 3D cultures can more accurately replicate the cell-to-cell interactions and extracellular environment found in vivo (Jensen, & Teng, 2020). A model of the brain using patient derived hiPSCs in a 3D culture would have both the same genetics as humans and also mimic the cell-to-cell interactions and extracellular environment found in animal models.

Bioprinting is the incorporation of living cells into biocompatible materials (Bishop *et al.* 2017). Typically, cells are incorporated into bioink, then printed using a bioprinter into a 3D construct. Computer aided design (CAD) is commonly used to design the structure of the bioprinted constructs. The most common types of bioprinting are inkjet, laser assisted and extrusion bioprinting. While inkjet and laser assisted bioprinting have higher resolution, extrusion bioprinting is faster, allows for the use of multiple bioinks at once, and allows for the use of different types of bioinks (Ozbolat & Hospodiuk, 2016). One issue with extrusion based bioprinting is the potential for large amounts of shear stress on the cells which can lead to decreased cell viability. Coaxial flow can be used to reduce this stress. Coaxial flow is where one material forms a sheath around an inner material (Kjar *et al.*, 2021). This sheath reduces the shear stress on the inner material.

Hydrogels are a common material used for bioinks. Hydrogels are hydrophilic polymers which can hold a large amount of water (Bahram *et al.,* 2016). Because these polymers are chemically crosslinkable the hydrogel is able to hold its structure. A common base for hydrogel bioinks is fibrin (Beyer *et al.*, 2013). Fibrinogen is a soluble protein that is found in the blood and upon conversion to fibrin will crosslink to form blood clots (Weisel & Litvinov, 2017). Fibrin is useful in bioinks as it is biocompatible and is able to be chemically crosslinked using thrombin. Cells are able to adhere to fibrin as it has cell binding sites (Nicolas *et al.*, 2020). In this way fibrin is able to mimic the *in vivo* extracellular matrix (ECM) (De Melo, *et al.* 2020). Without this property the embedded cells would undergo detachment mediated apoptosis (Science Direct. (n.d.). Fibrin however has a weak structure. This can be amended by the addition of other polymers such as alginate, another common hydrogel base (Beyer *et al.*, 2013; Nicolas *et al.*, 2020). Alginate is an unbranched polysaccharide found in brown algae. Alginate is

cheap to produce, non-toxic and is able to be chemically crosslinked using divalent cations such as Ca^{2+} (Bahram *et al.,* 2016; Lee *et al.*, 2012; Datta *et al.,* 2019). When mixed with fibrin in different ratios the physical properties of the bioink change. This is important as the components and stiffness of the matrix that NPC's are suspended in can have an impact on the course of their differentiation.

Our lab has shown that fibrin hydrogels support neuronal differentiation of hiPSCs, increase viability, and encourage neurite outgrowth (Abelseth *et al.* 2019). We have also found that the addition of genipin stabilizes fibrin hydrogels and encourages neurite outgrowth in hiPSC derived neurons (Robinson *et al.,* 2017). Our lab has created a novel fibrin based bioink including chitosan and alginate that is crosslinked by a solution containing thrombin, genepin, and calcium chloride (Abelseth *et al.* 2019; De la Vega *et al.,* 2018). Thrombin first cleaves fibrinogen, turning it into fibrin (Weisel & Litvinov, 2013). Ca^{2+} promotes the polymerization of the fibrin. Alginate also crosslinks in the presence of Ca^{2+} (Lee & Mooney, 2012). Chitosan and fibrin are then crosslinked by genipen (Schek *et al.,* 2011; Dimida *et al.*, 2017).

Our bioink has been used in conjunction with the RX1 bioprinter from Aspect Biosystems and their lab on a printer microfluidic printhead to print mature neural tissues from hiPSC derived NPC's (De la Vega *et al.,* 2018). The RX1 bioprinter is an extrusion based bioprinter which uses coaxial flow to reduce shear stress (Thomas, & Willerth, 2017; Beyer *et al.* 2014). In the case of the lab on a printer technology, the crosslinker wraps around the cell laden bioink from both sides. This outer sheath protects the cells from shear stress (Beyer *et al.* 2014).

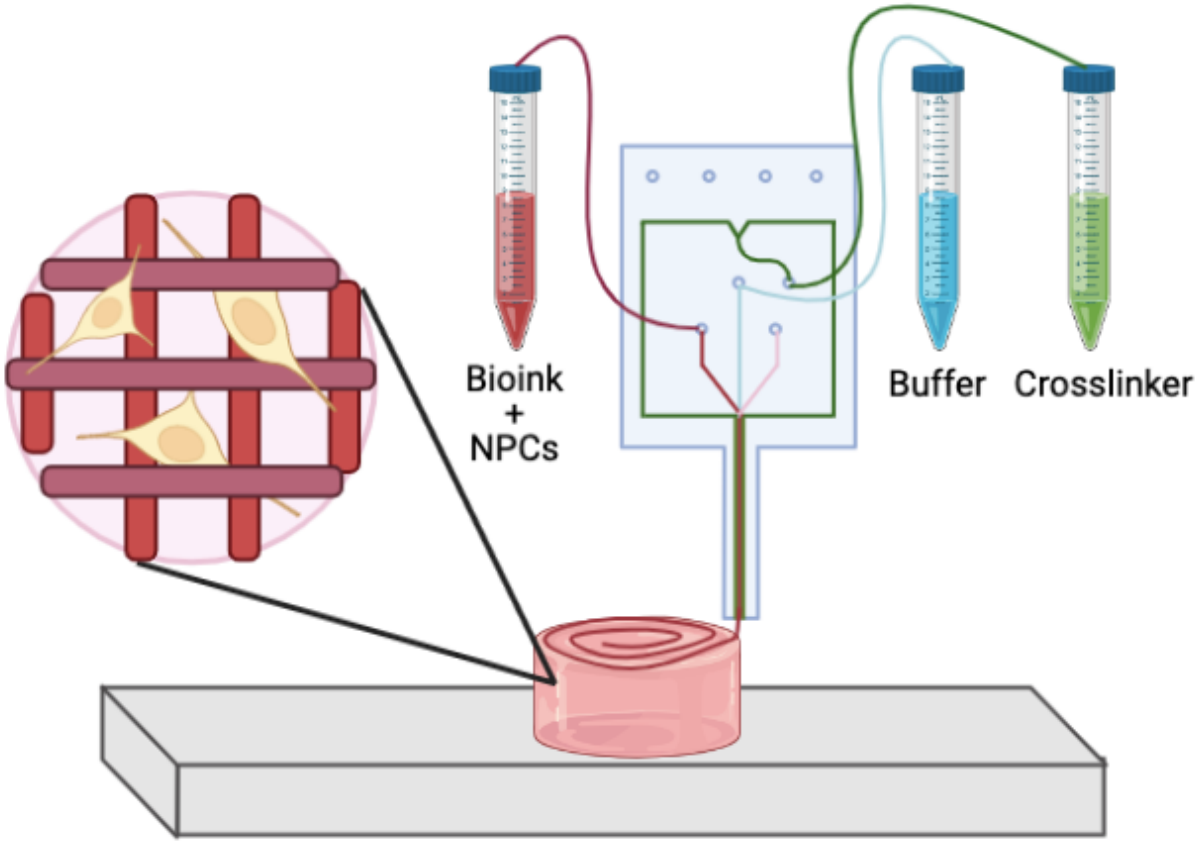

Figure 3: Process of 3D bioprinting neural tissue using our lab's bioink and the lab on a printer microfluidic printhead from Aspect biosystems.

Neural progenitor cell laden bioink combines with crosslinker and buffer and is extruded onto the printing surface. The printhead is moved in concentric circles while moving up in layers to create a ring structure. Magnification shows NPC's in the matrix formed by cross linked fibrin, alginate and chitosan.

1.7 Hypothesis and Objectives:

We believe a 3D printed model of AD using our lab's fibrin-based bioink and patient derived hiPSCs could be a more accurate model of AD than either animal or 2D cell culture

models. The first step in creating this model is showing that our lab's bioink can support our patient derived hiPSC derived NPC's and their differentition into cortical neurons. To show neural development we will stain the cells with the early neuronal cytoskeleton marker beta tubulin III (Tuj-1) and the nuclear marker DAPI and image the constructs using confocal microscopy to show neurite outgrowth. Successfully differentiated neurons should have both neurites and stain positive for Tuj-1.This study aims to begin to characterize this model before the eventual goal of its in drug screening and AD research

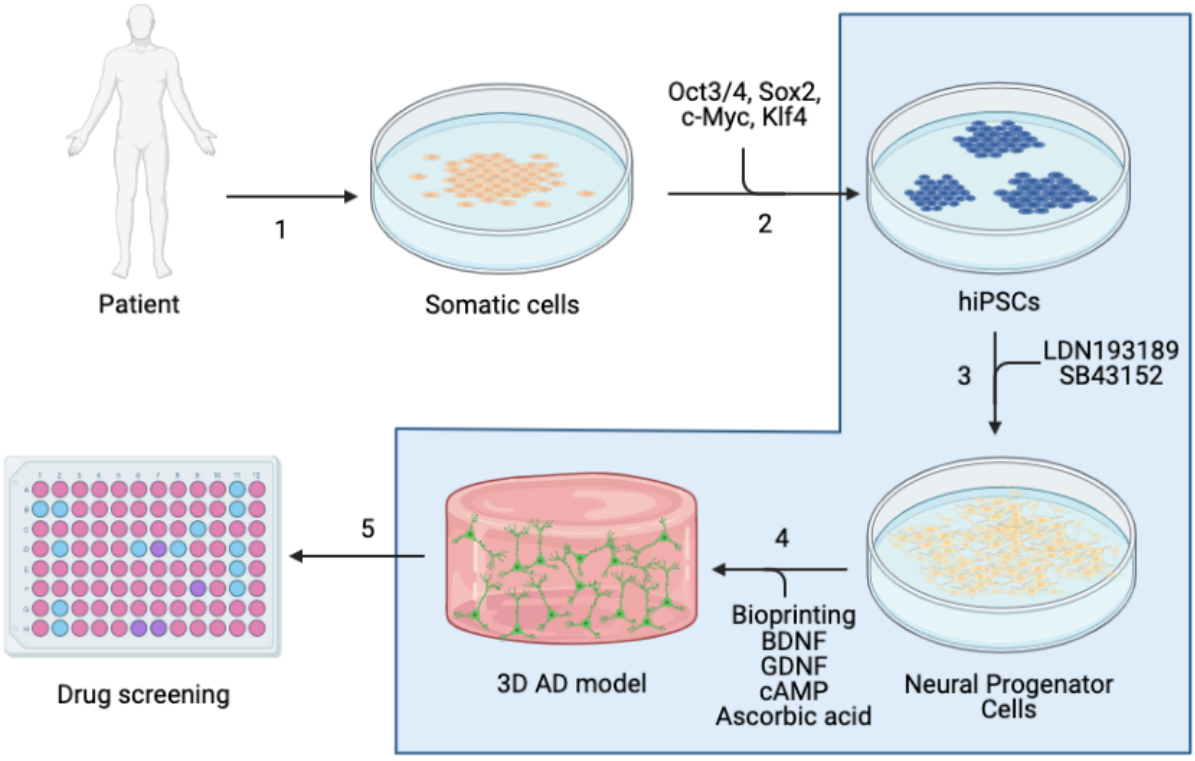

Figure 4: Process from patient to drug screening using patient derived human induced pluripotent stem cells.

(1) Retrieval of peripheral blood or fibroblasts from an AD patient. (2) Induction of pluripotency using the Oct3/4, Sox2, c-Myc, and Klf4. (3) neural induction with the dual SMAD inhibition protocol using LDN193189 and SB43152. (4) Bioprinting of NPC's and differentiation of NPC's

into into cortical neurons into BDNF, GDNF, cAMP, and ascorbic acid. (5) Use of the 3D AD model to screen for new disease modifying drugs. Highlighted area indicates the course of this project.

Chapter 2: Methods and Materials

2.1 Materials

DMEM/F12 + Glutamine media, Neurobasal media, N2 Supplement, B27 Supplement, GlutaMax, Insulin-Transferrin-Selenium-Sodium, Pyruvate, and Versene were purchased from Gibco. (Waltham, MA, USA). 2-Mercaptoethanol, Non-Essential Amino Acids Solution, primary mouse antibody anti-TUJ1, Alexa Fluor® 488 goat anti-mouse antibody, 4′,6-diamidino-2-phenylindole (DAPI), amyloid beta 40 human ELISA kit, ultrasensitive amyloid beta 42 human ELISA kit, cell extraction buffer, and CultureOne supplement were purchased from Thermo Fisher (Waltham, MA, USA). Penicillin/streptomycin, DMSO, SB431542, LDN193189, human basic fibroblast growth factor (bFGF), Tris(hydroxymethyl)aminomethane (Tris Base), sodium alginate, chitosan, β-Glycerophosphate disodium salt hydrate (β-GP), genipin, lyophilized thrombin, triton-X (T-X), AEBSF, protease inhibitor cocktail, normal goat serum (NGS) and calcium chloride were purchased from Sigma Aldrich (St. Louis, MO, United States). mTeSR-1 media, ReLeSR, BrainPhys Medium, 50X SM1 supplement, 100X N2-A supplement, and ascorbic acid were purchased from Stemcell Technologies (Vancouver, BC, Canada) NaCl and acetic acid were purchased from Caledon Laboratory Chemicals (Georgetown, ON, Canada). Y-27632, cyclic AMP, accutase solution, and lyophilized fibrinogen were purchased from EMD Millipore (Burlington, MA, USA). Matrigel was purchased from Corning (NY, USA). Tris HCl was purchased from Biobasic Canada (Markham, ON, Canada). KCl was purchased from ACP Chemicals (Montreal, QC, Canada). Brain derived neurotrophic factor (BDNF) & glial derived neurotrophic factor (GDNF) were purchased from Cedarlane Laboratories (Burlington, MA, USA).

Media formulations:

Basal neural maintenance medium (BNMM):

- 1:1 ratio of DMEM/F12 + Glutamine media (Gibco, Waltham, MA, USA) and Neurobasal media (Gibco, Waltham, MA, USA),
- 0.5% v/v N2 supplement
- 0.5% v/v N2 Supplement (Gibco, Waltham, MA, USA),
- 1% v/v B27 Supplement (Gibco, Waltham, MA, USA),
- 0.5% v/v GlutaMax (Gibco, Waltham, MA, USA),
- 0.5% v/v Insulin-Transferrin-Selenium-Sodium Pyruvate (Gibco, Waltham, MA, USA)
- 0.08% v/v 2-Mercaptoethanol (Thermo Fisher, Waltham, MA, USA),
- 0.5% v/v Non-Essential Amino Acids Solution (Thermo Fisher, Waltham, MA, USA),
- 1% v/v penicillin streptomycin (Sigma Aldrich St. Louis, MO, United States

Brain Phys + Culture One (BP+C1):

- BrainPhys Medium (Stemcell Technologies, Vancouver, BC, Canada),
- 2% v/v 50X SM1 supplement (Stemcell Technologies, Vancouver, BC, Canada),
- 1% v/v 100X N2-A supplement (Stemcell Technologies, Vancouver, BC, Canada),
- 1% v/v 100 mg/mL cAMP (EMD Millipore Burlington, MA, USA) ,
- 200 nM ascorbic acid (Stemcell Technologies, Vancouver, BC, Canada),
- 1% v/v CultureOne supplement (Thermo Fisher, Waltham, MA, USA)
- 1% v/v penicillin/ streptomycin (Thermo Fisher, Waltham, MA, USA)

Brain Phys +-Culture One (BP-C1):

- BrainPhys Medium
- 2% v/v 50X SM1 supplement
- 1% v/v 100X N2-A supplement
- 1% v/v 100 mg/mL cAMP
- 200nM ascorbic acid
- 1% v/v penicillin/streptomycin

Brain Phys - Culture One – ascorbic acid- cAMP (BP-C1-A.A-cAMP);

- BrainPhys Medium
- 2% v/v 50X SM1 supplement
- 1% v/v 100X N2-A supplement
- 1% v/v P/S

2.2 hiPSC Cell lines:

The two patient derived hiPSC's cell lines used were from the Haakon Nygaard lab at the University of British Columbia. The "ADAPP" cell line comes from a female patient with the fAD causing APP-London (V717I) mutation. The control "HN1" line comes from the male spouse of the patient. The use of these cell lines has been approved by the UBC Clinical Research Ethics Board (H07-03022: Clinical and Laboratory Studies in Dementia).

2.3 hiPSC Cell Culture:

hiPSCs were cultured on Matrigel coated 6 well cell culture plates. The media used was mTeSR-1 media and was changed daily until 85-90% confluent. The cultures were supplemented with 10mM Y-27632 for the first 24 hours after plating. The hiPSC's were passaged in 50-100 cell aggregates using ReLeSR passaging reagent. Cells were stored in liquid nitrogen in 90% mTeSR-1, 10% DMSO plus 10mM Y-27632 freezing medium.

2.4 Neural Induction

Neural induction protocol was based on the dual SMAD inhibition protocol used by Rose *et al.* (2018).

The HN1 and ADAPP hiPSCs used for neural induction had passage numbers of 32 and 27 respectively. On day zero of neural induction 80% confluent wells of hiPSC' were passaged in a 3/1 ratio in 50-100 cell aggregates using ReLeSR passaging reagent. This was done on Matrigel coated six well plate in 3mL mTeSR-1 plus 10mM Y-27632. On day one to day seven of differentiation, neural induction medium (NIM)(BNMM + 10 μM SB431542 + 0.5 μM LDN193189 + 10 μM Y-27632) was used. On the eighth day, cells were lifted by bathing the cells in Versene for 5 minutes at 37°C. Versine was aspirated and 3 ml BNMM was added to the well. Cells were scraped off of the plate and seeded into three Matrigel coated wells in 50-100 cell aggregates. Starting on day nine, media was changed daily with neural stem cell (NSC) medium (BNMM + 20ng/mL bFGF) until day eleven. Phase contrast images were taken of NPC's on day

12 of their differentiation to observe neural rosettes. On day 16, media was switched to NSC medium + 10 μM Y-27632. The media was replaced every three days until day 23. On day 23, NPC's were washed with PBS and lifted with accutase solution for 10 min at 37℃. The NPC's were stored in liquid nitrogen in 90% BNMM, 10% DMSO freezing medium at 20 million cells per vial. Phase contrast images were taken of NPC's on day 12 of their neural induction the Leica DMI3000B microscope (Leica Biosystems, Wetzlar, Germany) and the QImaging RETIGA 2000R camera (QImaging, Surrey, BC, Canada) at 10X magnification.

2.5 Bioink Preparation:

Bioink was prepared, and constructs were printed and designed based on the procedure described in Abelseth *et al.* (2019).

Fibrin Preparation:

4L of Tris Buffered Saline Solution (TBS) (4.36% w/v, TrisHCl 0.64% w/v Tris Base, 8% w/v NaCl and 0.2% w/v KCl in deionized (DI) water). 185 mg of lyophilized fibrinogen was added to a 100mm petri dish. 3 mL of TBS was added to the fibrinogen. The fibrinogen in TBS was then incubated for 1-2 hours at 37°C until the fibrinogen was fully dissolved. The fibrinogen solutions were then dialyzed in 4L of TBS overnight. The fibrinogen solution was then sterile filtered with a 0.2mm syringe filter. The concentration of fibrinogen was then measured on a NanoVue Plus spectrophotometer. The final concentration of fibrinogen was then ensured to be approximately 50mg/mL.

Alginate Preparation:

A 2% alginate solution was prepared by adding sodium alginate to DI water. Alginate solution was then stirred overnight with a magnetic stir plate and stir bar to dissolve the sodium alginate.

Chitosan Preparation:

A 1% v/v acetic acid solution was made by adding acetic acid into DI water. While stirring with a magnetic stir plate and stir bar, the chitosan was added to the acetic acid solution to make a 2.5% w/v chitosan solution. The solution was stirred overnight to allow the chitosan to fully dissolve. The chitosan solution was then sterile filtered with a 0.2mm syringe filter. Chitosan was then autoclaved at 121℃ for 30 minutes. The pH of the chitosan was brought to between pH7 and pH 8 by adding a 56% w/v β-GP. The chitosan solution was then stored at 4°C and assumed to be 1.9% w/v.

Genipin and Thrombin Preparation:

DMSO was added to powdered genipin (Sigma Aldrich St. Louis, MO, USA) to make a 2.5% w/v solution. Sterile TBS was added to lyophilized thrombin to make a 1000 U/mL solution. Both solutions were stored at -20°C.

Calcium Chloride Preparation:

A 2.086% w/v solution of calcium chloride was prepared in TBS. The calcium chloride solution was then sterile filtered with a 0.2 um syringe filter and then stored at 4°C.

Crosslinker Preparation:

The previously prepared, 2.5% w/v genipin and 1000U/mL thrombin were added to the 2.086% w/v calcium chloride to create crosslinker solution with final concentrations of 2% w/v calcium chloride, 0.075% w/v genipin and 1.7U/mL thrombin. The crosslinker solution was then sterile filtered using a 0.2mm filter.

2.6 Incorporation of NPC's into bioink

Frozen NPC's of both ADAPP line and HN1 line were seeded with a ratio of one vial of NPC's to one Matrigel coated 6 well cell culture plate 1 week before printing. NPC's were expanded in the NSC medium. This medium was replaced daily. Phase contrast images were taken of NPC cultures on the day of bioprinting. Before printing NPC's were lifted by incubating in 1.5mL accutase per well for 10 minutes at 37℃. DMEM/f12 was added to collected accutase so the ratio was 1:1 accutase / DMEM/F12. The number of NPC's in solution were counted. 5 million cells per mL of bioink were collected. The calculated volume of cell mixture was centrifuged at 300rcf for 5 minutes. The supernatant was removed, and the cells were resuspended in a fibrin solution. The genipin and thrombin were mixed and sterile filtered using a 0.2mm filter. The TBS, genipin/thrombin solution and NPC fibrin solution were mixed and taken to print. The final

concentrations of each of the components were 20mg/mL fibrin, 0.5% w/v alginate, 0.3g/mL chitosan and 5 million NPC's/mL of bioink.

2.7 3D Printing

NPC's were printed on the RX1 bioprinter using the Lab on a Printer microfluidic printhead (Aspect Biosystems, Vancouver, BC, Canada). The ring structure printed was 8 layers high and 1cm in width. Once printed, the constructs were placed in a 12 well plate containing anti adherence rinsing solution (Stemcell Technologies, Vancouver, BC, Canada) and once all constructs were printed the anti-adherence rinsing solution was replaced with culture media.

2.8 Cortical Neuron Differentiation and Culture

100% media changes were done with 1mL of sterile filtered BP+C1 media on day 0 and 2. 50% medium changes were done on day 5, 8, 11, and 14 with BP+C1 media. On day 17 & 20, 50% media changes were done with BP-C1 media. All subsequent media changes were 50% media changes with BP-C1-A. A.-cAMP media. 0.2uL of 100 ug/mL brain derived neurotrophic factor & glial derived neurotrophic factor per 1 mL of BrainPhys medium was added fresh before every media change.

2.9 Immunocytochemistry (ICC) and Confocal Imaging

On day 45 the AD and control constructs were fixed using 10% Paraformaldehyde for 15 minutes. The constructs were permeabilized at room temperature in a 0.1M PBS, 20% v/v DMSO, and 2% v/v T-X solution. The constructs were stained for the early neuronal cytoskeleton marker Tuj-1. Constructs were blocked at room temperature in 0.1M PBS with 20% DMSO, 2% T-X, and 10% normal goat serum. Constructs were incubated for 4 days in 0.1M PBS with 20% DMSO, 2% T-X, and 2.5% NGS and a 1:500 dilution of primary mouse antibody anti-TUJ1 at room temperature. Constructs were washed four times for one hour at room temperature in 0.1M PBS with 20% DMSO and 2% triton X. the constructs were then incubated for two days at 4C in 0.1M PBS with 20% DMSO, 2% T-X, and 2.5% NGS and a 1:500 dilution of Alexa Fluor® 488 goat anti-mouse antibody. The constructs were then washed with PBS two times for 15 minutes at 4°C. The constructs were then stained with 1mg/mL DAPI for 10 minutes at room temperature. The constructs were then washed again with PBS 2 times for 15 minutes at 4°C. Confocal images were taken of the printed constructs using the FIPS – Zeiss Confocal Laser Scanning Microscope at 20x magnification. The excitation and emission wavelengths used for detecting Alexa Fluor 488 (Tuj-1) were 488 nm and 525 nm and for DAPI they were 358nm and 461nm.

2.10 Morphological Analysis of Neural Rosettes and Neurite Structures

Mean neural rosette diameter on day 12 of neural induction was measured using the ImageJ image processing software. Three neural rosettes each from three wells of a six well cell culture plate was measured (n = 9). This was done for both cell lines.

Neurite lengths were measured using the ImageJ image processing software (n = 3). This was done for both cell lines. Neuron characteristics (ie. dendritic spines, axonal boutons, axonal varicosities and arborization) were visually identified.

2.11 Statistical Analysis

Two sample t-tests were performed on the diameter of neural rosettes and the lengths of observed neurons significance was defined as $p < 0.05$. Standard error of the mean neural rosette diameter (n=3) calculated for each cell line. Standard error for neurite length (n=3) for the AD and control constructs.

Chapter 3: Results

3.1 Neural induction of hiPSCs

Control (HN1) and AD (ADAPP) hiPSCs were differentiated into NPC's. Figure 5 shows phase contrast images of individual wells of both the ADAPP and HN1 cell lines the 12th day of neural induction. In the culture of ADAPP NPC's, neural rosettes were present and covered approximately 70% of the wells. In the culture of HN1 NPC's neural rosettes were present and also covered approximately 70% of the well. ADAPP neural rosettes were less defined than those found in the HN1 cell line. The mean diameter of neural rosettes in ADAPP wells A1, A2, and A3 were 91.2µm, 104.8µm, 76.8µm respectively (table 1). The mean diameter of neural rosettes in HN1 wells H1, H2, and H3 were 33.2µm, 49.2µm, and 39.2µm respectively. The average diameter of neural rosettes in the ADAPP line was 91µm +/- 8.1. The average diameter of neural rosettes in the HN1 line was 41µm +/- 4.7. Using a two-sample t-test with a significance threshold of $p < 0.05$ it was found that the neural rosette diameter was significantly different between the two cell lines ($p=0.0028$)

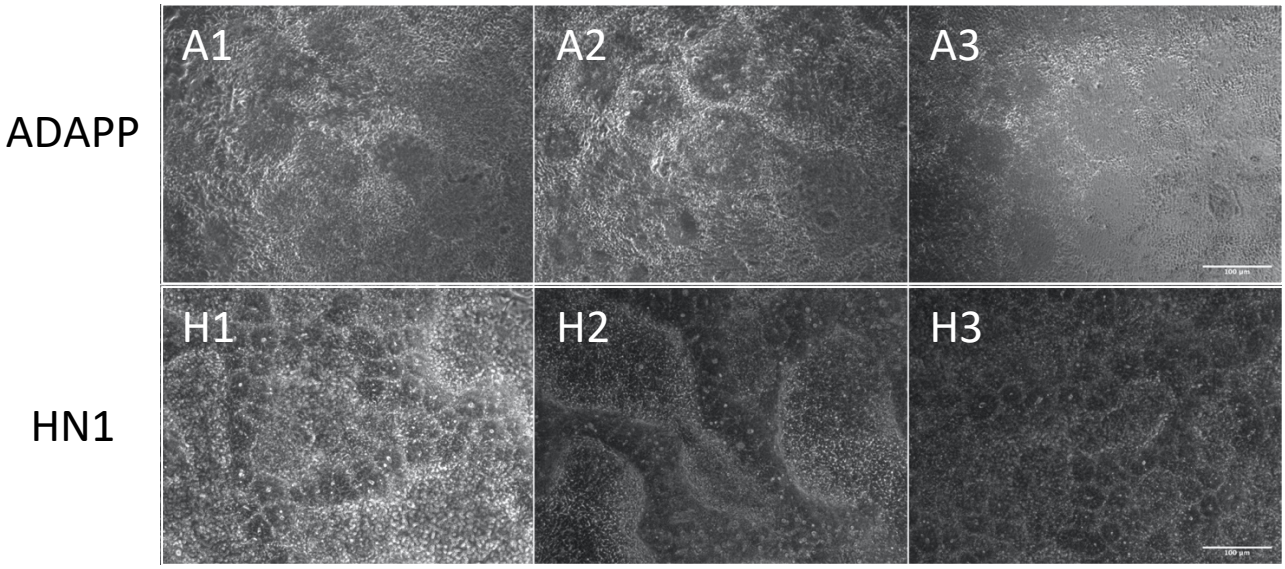

Figure 5: Phase contrast images of neural rosettes on Day 12 of neural induction of ADAPP (A1, A2, A3) and HN1 (H1, H2, H3) hiPSCs. Phase contrast images were taken of three separate wells of a 6 well cell culture plates containing ADAPP and HN1 cells on day 12 of neural induction. Neural rosettes covered approximately 70% of the wells in both cell lines. Images were taken at 20x magnification. Scale bar represents 100µm.

Table 1: Mean Neural rosette diameter and standard error was calculated from three randomly selected neural rosettes each from three wells of a six well cell culture plate. A Two sample t-test was conducted between the HN1 and ADAPP neural rosette diameter with a significance threshold of $p > 0.05$. It was found that the mean neural rosette diameters between the two cell lines were significantly different. ($p=0.0028$)

	1	2	3	Mean	Standard Error	T-test p value
ADAPP	91µm	105µm	77µm	91µm	8.1	0.0028
HN1	33µm	49µm	39µm	41µm	4.7	

3.2 Analysis of Control and AD Constructs

Control and AD constructs were 3D bioprinted using HN1 and ADAPP NPC's respectively. Using ICC and fluorescent confocal microscopy, cells in the AD 3D printed constructs stained positive for tuj-1 (green) and DAPI (blue) (figure 6, 7). Neurite extensions were observed in all three of the AD 3D printed constructs. Neurite lengths were measured to be 367µm (construct A), 127µm (construct B), 43µm (construct C) (Table 2). The average length was determined to be 179µm +/- 97. Axonal arborization was also present on the neurite in construct A (figure 6, I). Numerous axonal boutons were present on the neurite extension in construct A (figure 7, II). One axonal varicosity with a length of 65µm is present on this neurite (figure 7, III). The neurite in construct B shows the presence of dendritic spines (figure 7, IV) as well as dendritic arborization (figure 7, V). The neurite in construct C also showed the presence

of dendritic spines (figure 7, VI) as well as dendritic arborization (figure 7, VII). Connectivity between neurons was not observed in any of the constructs.

Using ICC and fluorescent confocal microscopy, cells in the control 3D printed constructs stained positive for tuj-1 and DAPI (figure 8, 9). Neurite extensions were observed in all three of the control constructs. Neurite lengths were measured to be 120µm (construct D), 166µm (construct E), 56µm (construct F) (table 2). The average length was determined to be 114µm +/- 32. An axonal bouton was present on the neurite in construct D (figure 9, VIII). The neurite in construct E shows the presence of axonal boutons (figure 9, IX) as well as axonal arborization (figure 9, X). the neurite in construct F also showed the presence of axonal arborization as well as (figure 9, XI) as well as a small second neurite (XII). Connectivity between neurons was not observed in any of the constructs.

Using a two sample t-test with a significance threshold of $p < 0.05$ it was found that the mean neurite length was not significantly different between the control and AD 3D printed constructs ($p=0.28$)(table 2).

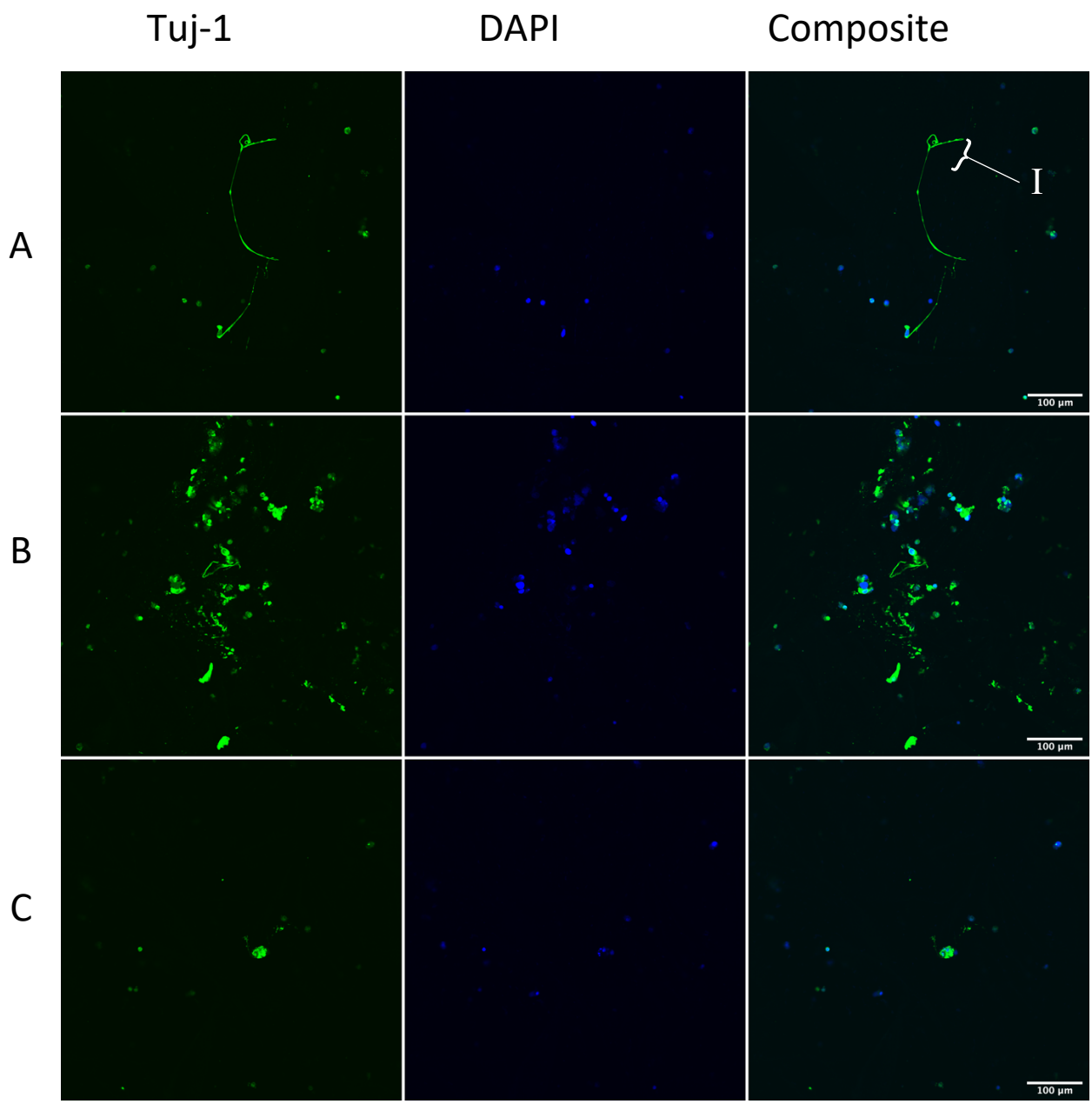

Figure 6: Fluorescent confocal immunocytochemistry images of 3D bio printed AD constructs. Cells were cultured for 45 days in a fibrin-based bio ink. A, B and C indicate individual 3D printed constructs. Constructs were stained for the early neuronal cytoskeleton marker tuj-1 (green) and the nuclear marker DAPI (blue). Images were taken with the FIPS – Zeiss Confocal Laser Scanning Microscope at 20x magnification. The excitation and emission wavelengths used

for detecting Alexa Fluor 488 (Tuj-1) were 488 nm and 525 nm and for DAPI they were 358nm and 461nm. (I) Axonal arborization on the neurite in in construct A. Scale bars represent 100µm.

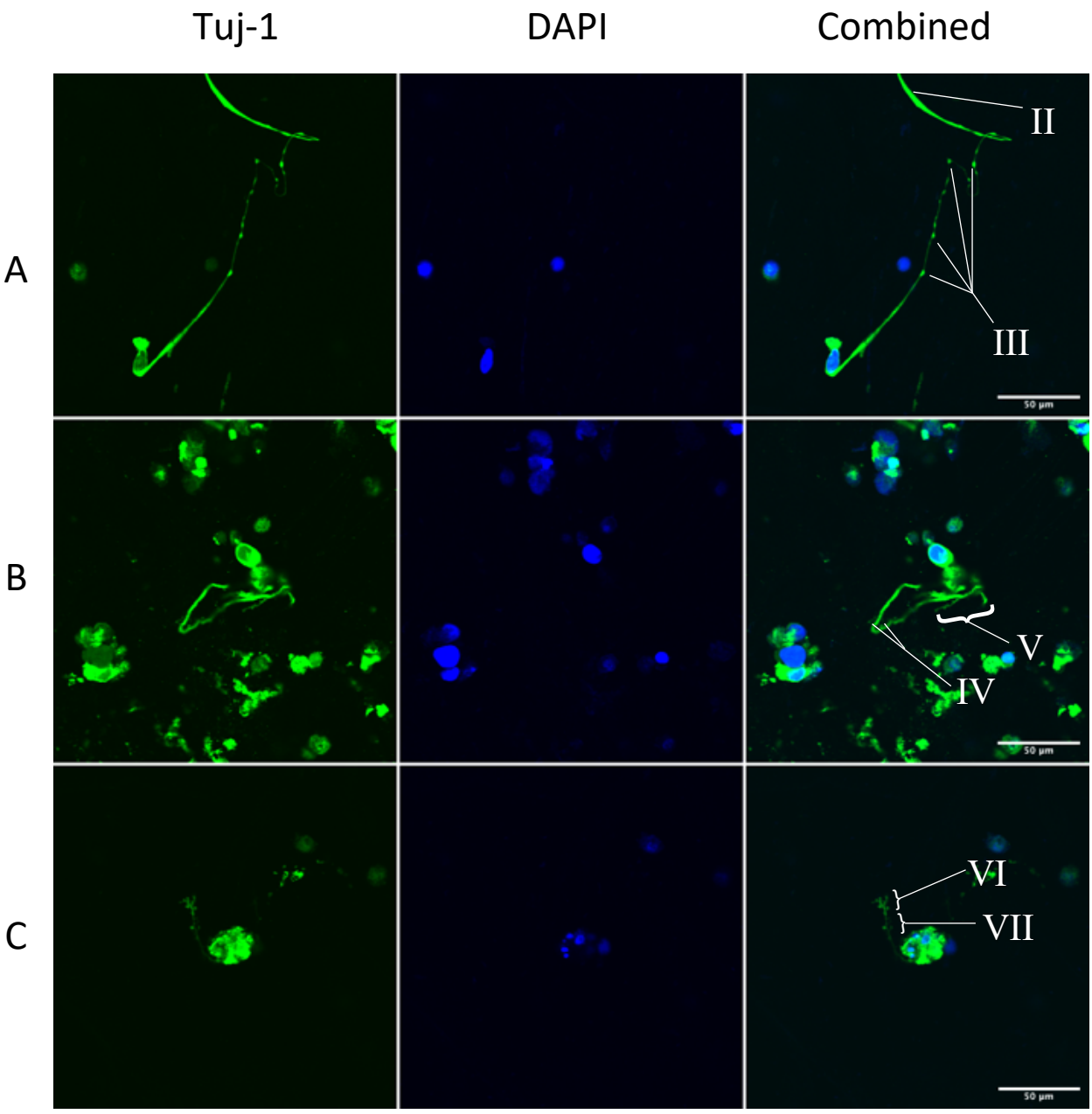

Figure 7: Fluorescent confocal immunocytochemistry images of 3D bio printed AD constructs. Cells were cultured for 45 days in a fibrin-based bio ink. A, B and C indicate individual 3D printed constructs. Constructs were stained for the early neuronal cytoskeleton marker tuj-1

(green) and the nuclear marker DAPI (blue). Images were taken with the FIPS – Zeiss Confocal Laser Scanning Microscope at 20x magnification +3x digital zoom. The excitation and emission wavelengths used for detecting Alexa Fluor 488 (Tuj-1) were 488 nm and 525 nm and for DAPI they were 358nm and 461nm. (II) 65 µm axonal varicosity on the neurite in construct A. (III) Axonal boutons on the neurite in construct A. (IV) Dendritic spines on the neurite in construct B. (V) Dendritic arborization on the neurite in construct B. (VI) Dendritic arborization on the neurite in in construct C. (VII) Dendritic spines on the neurite in construct C. Scale bars represent 50µm.

Table 2: Mean neurite lengths and standard error in AD control 3D bio printed constructs. Neurite lengths were measured using the ImageJ image processing program with fluorescent confocal images at 20x magnification. Mean neurite length and standard error were calculated for each line of cells. A Two sample t test was conducted between the control and AD neurite lengths with a significance threshold of $p > 0.05$. It was found that the mean neurite lengths were not significantly different. ($p=0.28$)

Neuron	**A**	**B**	**C**	**Mean**	**Standard Error**	**T-test p value**
ADAPP	367µm	127µm	43µm	179µm	97	
Neuron	**D**	**E**	**F**	**Mean**	**Standard Error**	0.28
HN1	120µm	166µm	56µm	114µm	31	

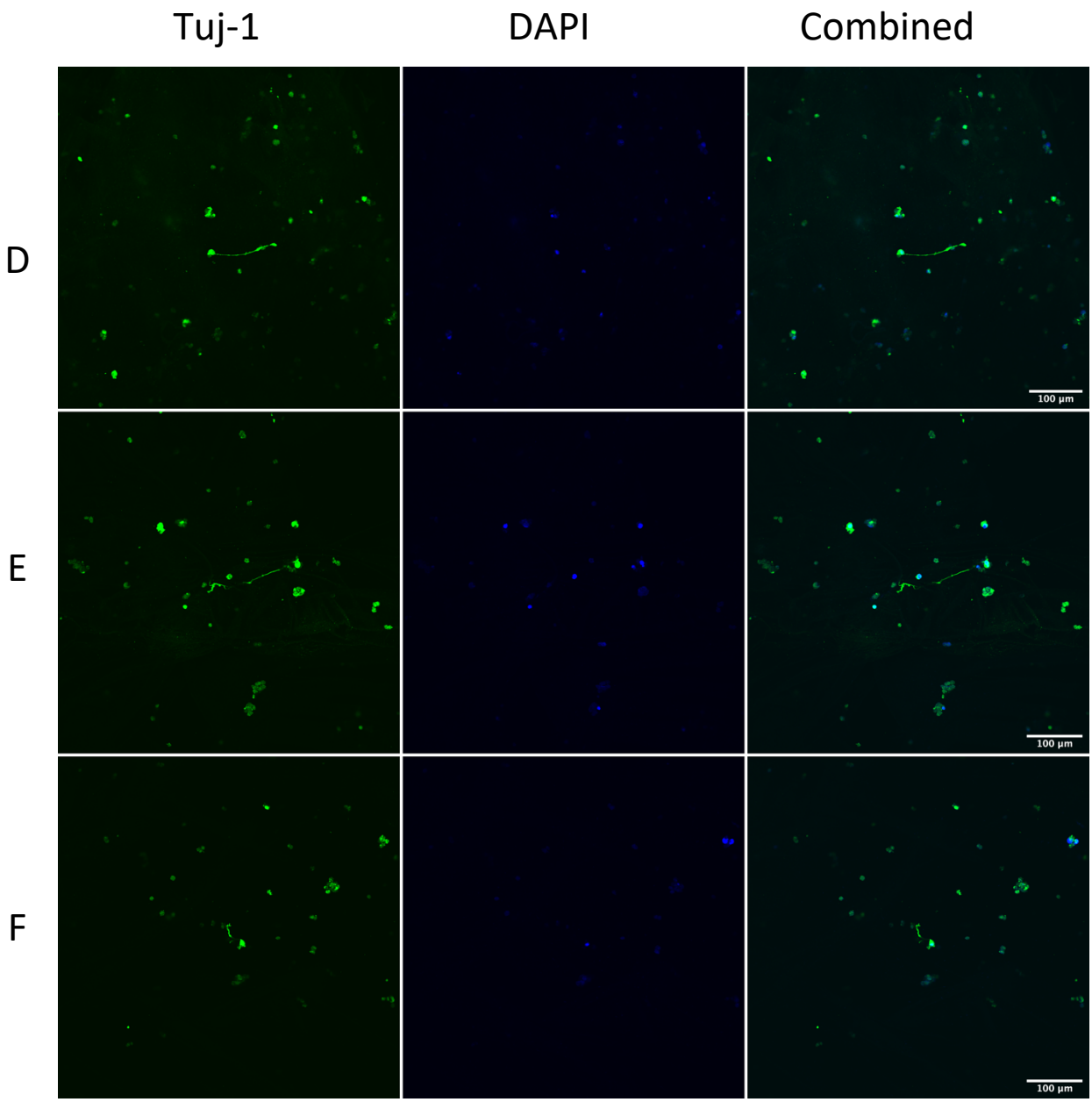

Figure 8: Fluorescent confocal immunocytochemistry images of 3D bio printed control constructs. Cells were cultured for 45 days in a fibrin-based bio ink. D, E and F indicate individual 3D printed constructs. Constructs were stained for the early neuronal cytoskeleton marker tuj-1 (green) and the nuclear marker DAPI (blue). Images were taken with the FIPS – Zeiss Confocal Laser Scanning Microscope at 20x magnification. The excitation and emission wavelengths used for detecting Alexa Fluor 488 (Tuj-1) were 488 nm and 525 nm and for DAPI they were 358nm and 461nm. Scale bars represent 100µm.

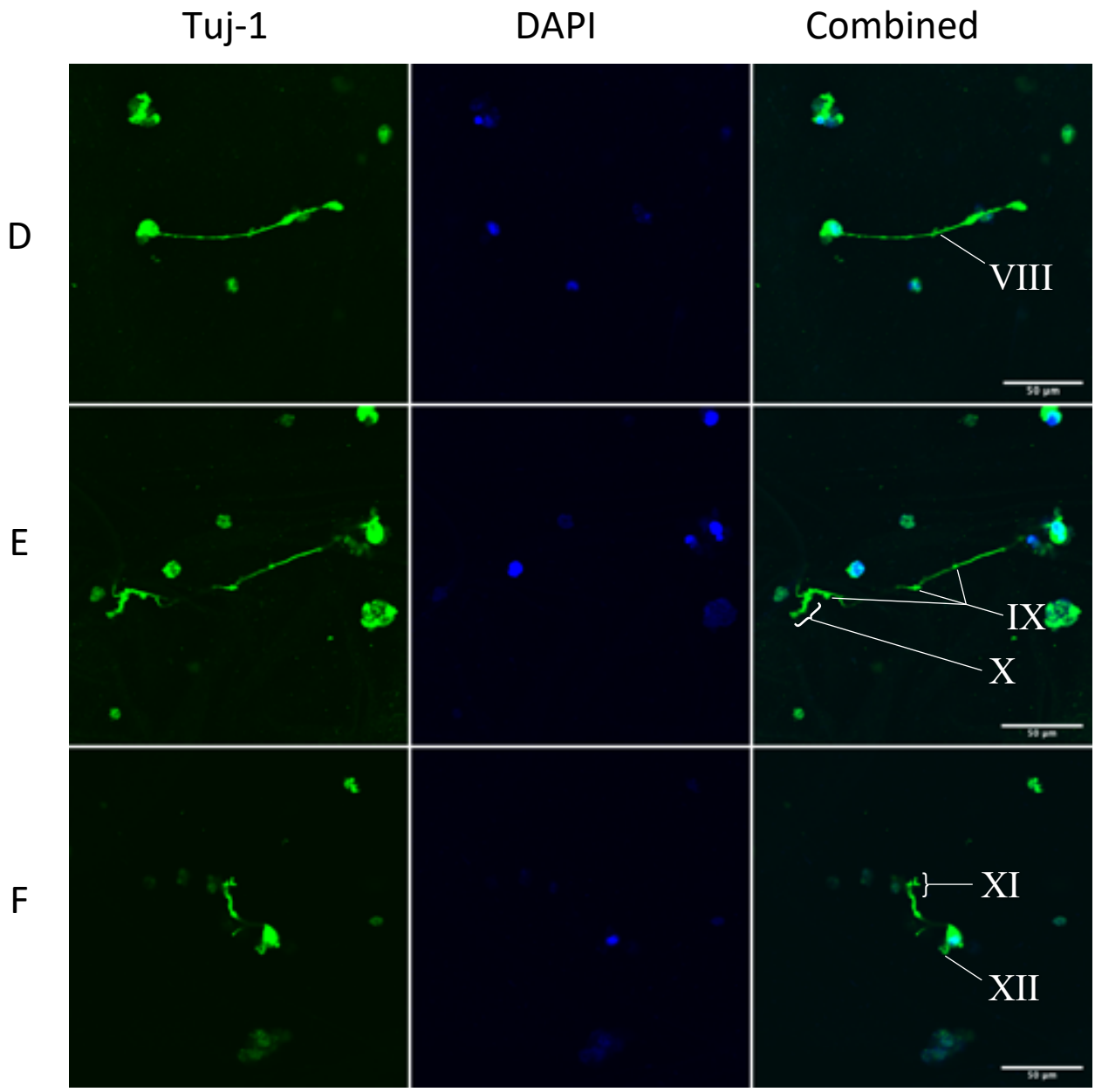

Figure 9: Fluorescent confocal immunocytochemistry images of 3D bio printed control constructs. Cells were cultured for 45 days in a fibrin-based bio ink. A, B and C indicate individual 3D printed constructs. Constructs were stained for the early neuronal cytoskeleton marker tuj-1 (green) and the nuclear marker DAPI (blue). Images were taken with the FIPS – Zeiss Confocal Laser Scanning Microscope at 20x magnification +3x digital zoom. The

excitation and emission wavelengths used for detecting Alexa Fluor 488 (Tuj-1) were 488 nm and 525 nm and for DAPI they were 358nm and 461nm. (VIII) Axonal bouton on the neurite in construct D. (IX) Axonal arborization on the neurite in construct E. (X) Axonal boutons on the neurite in construct E. (XI) Axonal/ dendritic arborization on the neurite in construct F. (XII) Secondary neurite on the cell in construct F. Scale bars represent 50µm.

Chapter 4: Discussion

4.1 Rationale

AD is a progressive neurodegenerative disease that affects tens of millions of people and represents a significant cost to healthcare systems around the world (Alzheimers Association, 2019; Sugitani *et al.,* 2002). Currently there are few drugs approved to treat AD, none of which slow or reverse the course of the disease (Alzheimer's Association, n.d.). The pathophysiology of the disease is not fully understood, although it is known that the aggregation of the proteins tau and Aß play a major role. Further research is needed to discover new pharmaceuticals and new aspects of the disease. The major models of AD used in the past have been animal and 2D cell culture models (Mangialasche *et al.,* 2010). These models have been instrumental in our current understanding of the disease and in the development of current AD treatments. However, animal models cannot replicate the relevant human physiology and genetics and 2D cell culture cannot reflect the 3D structure, extracellular environment or the cell-cell interactions found *in vivo* (Jensen, & Teng, 2020; Perlman, 2016).

The development of hiPSCs in 2006 opened up new avenues for disease modeling. Past work has shown that human cortical neurons can be created by successively differentiating hiPSCs into NPC’s using a dual SMAD signaling inhibition protocol. They can then be differentiated into cortical neurons using the small molecules BDNF, GDNF, cAMP and ascorbic acid in a 2D monolayer. These cultures have been shown to form neurite structures and the early

neuronal cytoskeleton marker Tuj-1 as well as other mature and cortical neuronal markers. (Frew *et al.,* 2020). Many studies have been published on differentiating fAD and healthy hiPSCs into cortical neurons in a 2D monolayer using patient derived hiPSCs and non-patient derived hiPSCs. When hiPSC lines are derived from a patient with fAD they can be used to model key aspects of the disease. fAD hiPSC derived neurons have been shown to accumulate and aggregate toxic amyloid beta oligomers and hyperphosphorylated tau (Lee *et al.,* 2020). However, as stated previously, these 2D cultures cannot reflect the 3D environment found *in vivo*.

Research on modeling AD using patient derived hiPSCs in 3D hydrogel cultures has been extremely limited and there has been no published research on modeling AD using 3D bioprinted hydrogel models. Our lab has developed a fibrin-based hydrogel bioink containing alginate and chitosan that is crosslinked by a solution containing calcium chloride, thrombin and genipen. In the past, our bioink has been used to successfully print hiPSC derived mature neural tissues using the RX1 bioprinter and lab on a printer microfluidic printhead (Abelseth *et al.* 2019; De la Vega *et al.,* 2018).

We believe that using fAD and healthy patient derived hiPSCs with the fAD, bioprinting using with our lab's fibrin based bioink, we can create a more physiologically relevant 3D model of AD that can be used for drug discovery and AD research. The first step in creating this novel model of AD is determining if our NPC's can survive and differentiate in our bioink. Differentiation of the NPC's was determined if the cells developed neurite processes in the bioink. This was also determined using immunocytochemical staining for the early neuronal

cytoskeleton marker tuj-1. On day 12 of neural induction neural rosettes were observed to confirm proper neural induction.

4.2 Findings

It was observed that the HN1 neural rosettes were more numerous and were smaller in size than the ADAPP line (figure 5, table 1). The ADAPP neural rosettes were larger and had less defined edges. To our knowledge no research has been published into why this may have been. The difference in neural rosette structure may have been a result of the different genetics between the two cell lines or because of different levels of hiPSC culture purity before the start of neural induction. This could also have been due to the hiPSCs used for neural induction being a high passage number. The HN1 and ADAPP line were passage number 32 and 27 respectively before neural induction. It has been found that hiPSCs at high passage numbers have more genetic mutations. This may have caused the different response in neural induction between the cell lines. However as neural rosettes were present in both cell lines it can be concluded that neural induction was successful.

After 45 days in 3D cortical neuron differentiation culture, the AD and control constructs were visually analyzed to evaluate the success of differentiation from the NPC's into neurons within the bioink. Our cells were cultured using a cocktail of the small molecules BDNF, GDNF, cAMP an ascorbic acid. We found that both lines of cells showed the formation of neurite processes (figures 6, 7, 8, 9). This indicates that the both the HN1 and ADAPP NPC's were successfully differentiated into neurons. This was confirmed using ICC. Both cell line neurons

stained positive for the early neuronal cytoskeleton marker Tuj-1 (Figures 6, 7, 8, 9). The length of the observed neurites was not observed to be significantly different between the two cell lines (table 2). Additionally, there was a significant amount of Tuj-1 expression in cells where neurites were not visible indicating that these cells had also successfully been differentiated into neurons. Due to the planar nature of confocal images, it is likely that there are neurites present on these cells, but they were not in the plane that the image was taken in. This can be confirmed in future work by creating a 3D Z-stack image with a confocal microscope. This would allow us to observe if there are additional neurites present. Differentiation into cortical neurons was not confirmed but could be confirmed in future work by staining for the cortical layer markers RELN (layer I) Brn-2 (layers II-VI) and Tbr-1 (layers V-VI) (Zhang *et al.,* 2018; Sugitani *et al.,* 2002; Meyer *et al.,* 2002).

We also observed that both the disease and healthy cells developed terminal and en passant axonal boutons, as well as dendritic spines on the neurite processes. These features are common on cortical neurons *in vivo.* Axonal boutons and dendritic spines form as a result of neuronal activity (Butz & van Ooyen, 2013). Their presence then suggests that the neurons differentiated in our model are electrically active. This further confirms the physiological relevance of our disease model. The activity of the neurons should be confirmed in future work using patch clamp recording.

Interestingly, the neurite on AD construct A showed a significant axonal swelling. Axonal swellings have been shown to be an effect of the accumulation of organelles within neurites in early in AD pathology (Stokin *et al.,* 2005). This suggests that the AD line of

differentiated neurons underwent early AD pathology. This could be confirmed in future work by staining for choline acetyltransferase as it accumulates within axonal swellings.

4.3 Other 3D Disease Models Using hiPSCs

Our lab has 3D printed hiPSC derived NPC's and successfully differentiated them into neurons within our bioink in the past (De la Vega *et al.,* 2018). De la Vega *et al.* also used dual inhibition of SMAD signaling to produce NPC's and printed using the RX1 bioprinter with the lab on a printer printhead. NPC's were also differentiated using a cocktail of BDNF GDNF, cAMP, and ascorbic acid with the addition of retinoic acid and puromorphine to induce differentiation into motor neurons. They found that their printed cells stained positive for Tuj-1 and that they were able form neurites. This indicates that the NPC's were successfully differentiated into neurons within the bioink. Their findings showed that our bioink is able to support and encourage neurite outgrowth of hiPSC derived NPC's (Abelseth *et al.,* 2019). Our work also confirms theirs which shows that healthy NPC's can successfully be printed and differentiated into neurons within our bioink. Our work however represents the first time that both diseased and healthy patient derived NPC's have successfully been differentiated in our bioink.

Salaris *et al.* used a 50% Matrigel 2% alginate bioink and patient derived hiPSCs in their 3D bioprinted cortical neural tissue model (2019). The researchers found that cells were able to form neurites and stained positive for the neuronal marker Tuj-1 as well as the deep layer cortical marker Tbr-1. Additionally, they observed connectivity between the neurons within their 3D

cultures. They also found that their neurons were functional using patch clamp recording. The lack of connections observed in our culture could be because the concentration of cells was not as high as in this study. The researchers noted that they used an increased the cell density (unspecified) to increase the visibility of the cells and decreased construct sizes (~3-5μL) to conserve cells used. If our cell density was not high enough the cells would then be unable to "find" each other to form synapses. It is also possible that there is connectivity between neurons in our model, but they are not viewable as they are not in the plane of the image. This could be confirmed in future work by making a 3D Z stack image which would allow us to see the connections between the neurons. This study corroborates our lab's work that 3D bio-printed NPC's are able to differentiate in a hydrogel bioink and that 3D bioprinting is a viable tool for modeling the brain. They have also definitively shown that cortical neurons are able to be differentiated in a hydrogel bioink.

To our knowledge ours is the first 3D model of AD that has employed the use of both bioprinting and patient derived hiPSCs. There has however been some research modeling AD in 3D using other methods of 3D culture.

Choi *et al.* (2014) has created a 3D model of AD using non-patient derived cells. The researchers used multiple fAD NPC lines containing mutations on the *APP* and *PSEN1* genes as well as an unmutated control line. In their model they differentiated NPC's into neurons within a Matrigel based hydrogel matrix. The constructs were created by pouring liquid Matrigel with incorporated cells into a cell culture plate where it then solidified. They then bathed the construct in differentiation media. They found that after 4-12 weeks of culture, the cells produced neurite

extensions and stained positive for the mature neuronal marker MAP2. This indicates that they were successfully differentiated into neurons. It was observed in this study that there were multiple neurons per image. This is likely because they used a Z stack 3D image allowing for the visualisation of neurons not exactly in the plane of the image. Using ICC and a western blot for Aß, they also found the AD cells had deposited Aß plaques while the control cells did not. The AD cells also stained positive for hyperphosphorylated tau within the soma and neurites. There findings support ours that both AD and healthy hiPSC derived NPC's are able to be differentiated into neurons in a hydrogel bioink. This also show that 3D cell culture models are a viable option for modeling the disease as they show both molecular hallmarks of the disease.

Hernández-Sapiéns *et al.* (2020) has created a 3D model of AD using patient derived hiPSCs suspended in Matrigel. The disease cell line used in this cell line used in this study carried the fAD causing mutation in the *PSEN1* gene as well as a non-mutated control cell line. They also used a dual SMAD inhibition protocol to produce their NPC's. NPC's were plated on top of a 3D Matrigel construct formed by using a cell culture dish as a mold. The 3D cultures were then bathed in culture medium. They found after 14 days of differentiation that the cells had developed neurite processes and stained positive for the neuronal markers Tuj-1 and MAP2 indicating successful differentiation into neurons. Their AD mutated line also stained positive for Aß while their non-mutated line did not. They performed a western blot for Aß and found that the AD line produced Aß monomers and oligomers while the non-mutated line did not. Their findings also support ours that it is possible to differentiate AD and healthy NPC's into neurons in a 3D hydrogel. Also, like Choi *et al.*, they have definitively shown an increase of Aß accumulation in AD cell lines.

Zhang *et al.* (2018) investigated the effect on AD on P21-activated kinase (pPAK) activity using a 3D AD model. In their model they used non-patient derived hiPSC derived NPC line with no fAD related mutations. AD pathology was induced by adding Aß oligomers to the culture medium. The researchers used a Puramatrix and laminin-based hydrogel scaffold for the 3D construct. They also ran their experiment in a 2D monolayer on poly-L-Ornithine and laminin coated plates. Their 2D and 3D models showed the presence of neurite process and stained positive for a number of neuronal and cytoskeleton markers indicating successful differentiation into neurons. They found a higher activity of pPAK in the 3D model compared to the 2D model. The addition of Aß oligomers in 3D modulated the localization of pPAK in the cell and had no effect in the 2D model. The redistribution of pPAK in response to Aß oligomers in the 3D culture matches the pathology observed *in vivo* while the pPAK response in the 2D culture did not. Their result support our findings that neurons can be successfully differentiated in a 3D hydrogel matrix. This also shows how 3D disease modeling can more accurately reflect the pathology of AD found in the human brain than a 2D culture can.

Papadimitriou *et al.* (2018) investigated synaptic plasticity in AD using hiPSCs and a 3D culture model using a starPEG-heparin-based hydrogel. The hiPSCs used in this paper did not have any mutations associated with fAD. They induced AD pathology by adding Aß 42 to the cultures. They observed the presence of neurite processes after 3 weeks in culture. The cells also stained positive for a variety of early neuronal cortical and mature neuronal markers confirming that they had been successful differentiated into cortical neurons. The found that the addition of Aß 42 to the culture increased the production of the enzyme KAT2. This has also been observed

in mouse models and in the human brain. Increased production of KAT2 has the effect of decreasing neuroplasticity of neurons. They found that the addition of Interleukin-4 restores to culture medium counters the effect of KAT2 and rescues the neural plasticity of the neurons. These results were confirmed using a 3D culture of primary neurons. In addition, they noted the presence of axonal boutons on the cultured neurons. It was not specified if these were terminal or en passant boutons. Their findings support ours that hiPSCs can be successful differentiated in a 3D hydrogel matrix. This also supports our finding that 3D cultured neurons can form bouton structures in a 3D culture. Their findings further demonstrate the ability of 3D hiPSCs models to accurately reflect AD pathology previously found in mouse models and in humans.

Though these studies have been successful at accurately modeling AD using hiPSCs , our model has a few key advantages over those reported here. Choi *et al.* (2014) and Hernández-Sapiéns *et al.* (2020) used a Matrigel based hydrogels. Matrigel gels are difficult to use as they need to be kept at low temperatures to avoid solidification. This is not the case with our fibrin based bioink. As a result, our model is easier to work with. In the model described in and Hernández-Sapiéns *et al.,* rather than suspending the cells in the hydrogel, cells were seeded on top of the Matrigel and allowed to grow into it. This is therefore not a true 3D model. In Papadimitriou *et al.* (2018), and Zhang *et al.* (2018), no cell line was used that had a fAD mutation. AD pathology was induced by adding Aß oligomers to the culture medium. This is a weaker representation of the disease than the use of fAD cell lines. Additionally, none of these models employed the use of bioprinting. Bioprinting allows for the easy incorporation of both AD and healthy cells to make a true 3D model of AD. It also allows for the creation constructs with a variety of shapes. This means that our cultures are not limited by the shape of the culture

dish used as a mold. Also, the only paper to note the presence of axonal boutons was Papadimitriou *et al.* and none of the studies observed dendritic spine structures or axonal swellings in the AD neurons. This is likely because the images used in our study are of higher quality than those taken in these studies and therefore more detail can be discerned. Dendritic spines and axonal swelling have been documented before in hiPSC cultures as well as in human brains (Butz & van Ooyen, 2013; Mariani *et al.,* 2012, Pchitskaya & Bezprozvanny, 2020, Sherriff *et al.,* 1994). This, however, is the first time they have been documented in a 3D AD model using hiPSCs. This further supports the fact that 3D models can accurately model diseased and healthy neural tissue.

4.4 Future Directions

Though our findings are promising for the future of our 3D AD model, more work is needed for it to be useful for AD research. Future work should confirm the development of the cells into cortical neurons by staining for the cortical layer markers factors RELN (layer I) Brn-2 (layers II-VI) and Tbr-1 (layers V-VI) as described in past publications (Zhang *et al.,* 2018; Sugitani *et al.* 2002; Meyer *et al.* 2002). Additionally, staining should be done for choline acetyl transferase to confirm the presence of axonal boutons as well as axonal swellings. This would work to validate the model's relevance to cortical brain regions. Additionally, the use of 3D Z stack images would be advantageous as they would allow us to view multiple neurons at once and allow us to see the connections between neurons. This could also be achieved by using higher cell densities, as described in Salaris *et al.* (2019). Higher cell density would increase the chance of viewing a neuron in the plane of the confocal microscope.

Future work should also show that the AD cells in our model deposit Aß plaques, oligomers and hyperphosphorylated tau as described in the previously described 3D AD models (Choi *et al.*, 2014; Hernández-Sapiéns *et al.,* 2020; Papadimitriou *et al.*, 2018). This could be done by staining for Aß or using a western blot. Additionally, future work should also be done to confirm that the AD cells have an increased Aß 42/40 ratio compared to the control line. This could be done using and Enzyme Linked Immunosorbent Assay (ELSIA) for both Aß 42 and 40. This would be the first 3D hydrogel model to show this increased ratio and would greatly increase the relevance of our AD model.

One of the weaknesses of this study is that in the human brain, along with neurons, there are many kinds of glial cells that support the neurons (Jakel & Dimou, 2017). Glial cells function as immune cells, support cells and myelinating neurons. Glial cells have been implicated in AD pathology (Kim *et al.,* 2018). It is clear then that their inclusion as a co-culture with our neurons is necessary to create a fully accurate model of AD. Another weakness that this study has is a lack of genetic diversity. Only one *APP* mutation from a single patient was used along with a genetically unrelated control. To fully validate this model, an assortment of cell lines with different fAD causing mutations should be used from different patients whose genetics will differ as seen in Choi *et al.* 2014). In addition, isogenic control lines should be generated which have the mutated genes knocked out in order to give a fully accurate control. The largest weakness of this model is that currently, only fAD can be modeled using this method as it has a genetic origin. However, fAD only makes up ~1% of all AD cases. Future work should attempt to further develop this model for sAD research.

4.5 Conclusions

Here we have shown the first steps in creating this model. We have shown that both AD and control patient derived hiPSCs are able to successfully differentiate within our bioink. We have also observed dendritic spines and axon swelling structures previously unobserved in 3D hydrogel models of the disease. These findings fit withing the growing body of research which shows that modeling using hiPSCs and 3D hydrogels is a promising avenue for modeling AD. This is also the first time that both patient derived hiPSCs and bioprinting have been used in conjunction to model AD. Once our model has been fully described, it has the potential to be an invaluable tool in the search for new drugs to treat AD and in AD research. In the future, this model can be used alongside animal and 2D cell culture models and eventually could replace them altogether.

References

Abelseth, E., Abelseth, L., De La Vega, L., Beyer, S. T., Wadsworth, S. J., & Willerth, S. M. (2019). 3D printing of Neural tissues derived from human induced pluripotent stem cells using A Fibrin-based bioink. *ACS Biomater, 5*(1), 234-243. doi:10.1021/acsbiomaterials.8b01235.s001

Alonso , A., Zaidi, T., Novak, M., Grundke-Iqbal, I., & Iqbal, K. (2001). Hyperphosphorylation induces self-assembly of tau into tangles of paired helical filaments/straight filaments. *Proceedings of the National Academy of Sciences of the United States of America*, *98*(12), 6923–6928. doi.org/10.1073/pnas.121119298

Alonso, A. D., Grundke-Iqbal, I., & Iqbal, K. (1996). Alzheimer's disease hyperphosphorylated tau sequesters normal tau into tangles of filaments and disassembles microtubules. *Nature Medicine, 2*(7), 783-787. doi:10.1038/nm0796-783

Alonso, A. D., Grundke-Iqbal, I., Barra, H. S., & Iqbal, K. (1997). Abnormal phosphorylation of tau and the mechanism of Alzheimer Neurofibrillary degeneration: Sequestration OF Microtubule-associated proteins 1 and 2 and the disassembly of Microtubules by the abnormal tau. *Proceedings of the National Academy of Sciences, 94*(1), 298-303. doi:10.1073/pnas.94.1.298

Alzheimer's Association. (n.d.). Medications for memory. Retrieved March 13, 2021, from https://www.alz.org/alzheimers-dementia/treatments/medications-for-memory

Alzheimers Association. (2019). 2019 Alzheimer's disease facts and figures. *Alzheimer's & Dementia, 15*(3). doi:10.1016/j.jalz.2019.01.010

Anderson, J. P., Esch, F. S., Keim, P. S., Sambamurti, K., Lieberburg, I., & Robakis, N. K. (1991). Exact cleavage site of alzheimer amyloid precursor in neuronal pc-12 cells. *Neuroscience Letters, 128*(1), 126-128. doi:10.1016/0304-3940(91)90775-o

Arber, C., Lovejoy, C., & Wray, S. (2017). Stem cell models of alzheimer's disease: Progress and challenges. *Alzheimer's Research & Therapy, 9*(1). doi:10.1186/s13195-017-0268-4

Armstrong, R. A. (2010). Risk factors for alzheimer's disease. *Dementia, 57*(2), 428-434. doi:10.1201/b13196-62

Bahram, M., Mohseni, N., & Moghtader, M. (2016). An introduction to Hydrogels and some recent applications. *Emerging Concepts in Analysis and Applications of Hydrogels*. doi:10.5772/64301

Baker, M. (2008). Embryoid bodies get organized. *Nature Reports Stem Cells*. doi:10.1038/stemcells.2008.146

Barbier, P., Zejneli, O., Martinho, M., Lasorsa, A., Belle, V., Smet-Nocca, C., Tsvetkov, P. O., Devred, F., & Landrieu, I. (2019). Role of Tau as a Microtubule-Associated Protein: Structural and Functional Aspects. *Frontiers in aging neuroscience*, *11*, 204. doi.org/10.3389/fnagi.2019.00204

Barker, R. A. (2017). The role of tau in Huntington's disease. *Alzheimer's & Dementia, 13*(7), 595-603. doi:10.1016/j.jalz.2017.07.401

Bayer, T. A., Cappai, R., Masters, C. L., Beyreuther, K., & Multhaup, G. (1999). It all sticks together—the app-related family of proteins and alzheimer's disease. *Molecular Psychiatry, 4*(6), 524-528. doi:10.1038/sj.mp.4000552

Beyer, S. T., Bsoul, A., Ahmadi, A., & Walus, K. (2013). 3D alginate constructs for tissue engineering printed using a coaxial flow focusing microfluidic device. *Institute of Electrical and Electronics Engineers,* 1206-1209. doi:10.1109/transducers.2013.6626990

Beyer, S.T, Walus, K., Mohamed, T., Bsoul. A.A.M. (2014). *System for additive manufacturing of three-dimensional structures and method for same* (United States of America US 2016/0136895). United States Patent and Trademark Office. https://patentimages.storage.googleapis.com/80/90/14/f64f2a9e16b3a9/US20160136895A1.pdf

Bierer, L. M., Hof, P. R., Purohit, D. P., Carlin, L., Schmeidler, J., Davis, K. L., & Perl, D. P. (1995). Neocortical neurofibrillary tangles correlate with dementia severity in Alzheimer's disease. *Archives of Neurology, 52*(1), 81-88. doi:10.1001/archneur.1995.00540250089017

Bishop, E. S., Mostafa, S., Pakvasa, M., Luu, H. H., Lee, M. J., Wolf, J. M., Ameer, G. A., He, T., & Reid, R. R. (2017). 3-D bioprinting technologies in tissue engineering and regenerative medicine: Current and future trends. *Genes & Diseases, 4*(4), 185-195. doi.org/10.1016/j.gendis.2017.10.002

Boularaoui, S., Al Hussein, G., Khan, K. A., Christoforou, N., & Stefanini, C. (2020). An overview of extrusion-based bioprinting with a focus on induced shear stress and its effect on cell viability. *Bioprinting, 20*. doi:10.1016/j.bprint.2020.e00093

Busche, M.A., Hyman, B.T. (2020). Synergy between amyloid-β and tau in Alzheimer's disease. *Nature Neuroscience* 23, 1183–1193. doi.org/10.1038/s41593-020-0687-6

Butz, M., & van Ooyen, A. (2013). A simple rule for dendritic spine and axonal bouton formation can account for cortical reorganization after focal retinal lesions. *PLoS Computational Biology, 9*(10), 3259-3259. doi.org/10.1371/journal.pcbi.1003259

Chambers, S. M., Fasano, C. A., Papapetrou, E. P., Tomishima, M., Sadelain, M., & Studer, L. (2009). Highly efficient Neural conversion of human ES and iPS cells by dual inhibition of Smad signaling. *Nature Biotechnology, 27*(3), 275-280. doi:10.1038/nbt.1529

Chambers, S. M., Qi, Y., Mica, Y., Lee, G., Zhang, X., Niu, L., Bilsland, J., Cao, L., Stevens, E., Whiting, P., Shi, S., & Studer, L. (2012). Combined small-molecule inhibition accelerates developmental timing and converts human pluripotent stem cells into nociceptors. *Nature Biotechnology, 30*(7), 715-720. doi.org/10.1038/nbt.2249

Chen, G., Xu, T., Yan, Y., Zhou, Y., Jiang, Y., Melcher, K., & Xu, H. E. (2017). Amyloid beta: Structure, biology and structure-based therapeutic development. *Acta Pharmacologica Sinica, 38*(9), 1205-1235. doi:10.1038/aps.2017.28

Chertkow, H., Feldman, H. H., Jacova, C., & Massoud, F. (2013). Definitions of dementia And predementia states in Alzheimer's disease and vascular cognitive impairment: Consensus from the Canadian conference on diagnosis of dementia. *Alzheimer's Research & Therapy, 5*(1). doi:10.1186/alzrt198

Choi, S. H., Kim, Y. H., Hebisch, M., Sliwinski, C., Lee, S., D'Avanzo, C., Chen, H., Hooli, B., Asselin, C., Muffat, J., Klee, J. B., Zhang, C., Wainger, B. J., Peitz, M., Kovacs, D. M., Woolf, C. J., Wagner, S. L., Tanzi, R. E., & Kim, D. Y. (2014). A three-dimensional human neural cell culture model of Alzheimer's disease. *Nature, 515*(7526), 274-293. doi.org/10.1038/nature13800

Choy, R. W., Cheng, Z., & Schekman, R. (2012). Amyloid precursor protein (app) traffics from the cell surface via endosomes for amyloid β (aβ) production in the trans-golgi network. *Proceedings of the National Academy of Sciences, 109*(30), 2077-2082. doi:10.1073/pnas.1208635109

Cook, D. G., Iwatsubo, T., Doms, R. W., Leight, S., Forman, M. S., Kolson, D. L., Lee, V. M. - Y., & Sung, J. C. (1997). Alzheimer's Aβ (1-42) is generated in the endoplasmic reticulum/intermediate compartment of NT2N cells. *Nature Medicine, 3*(9), 1021-1023. doi.org/10.1038/nm0997-1021

Datta, S., Barua, R., & Das, J. (2019). Importance of alginate Bioink for 3D Bioprinting in tissue engineering and regenerative medicine. *Alginates - Recent Uses of This Natural Polymer*. Intechopen.

De la Vega, L., A. Rosas Gómez, D., Abelseth, E., Abelseth, L., Allisson da Silva, V., & Willerth, S. (2018). 3D bioprinting human induced pluripotent stem cell-derived neural tissues using a novel lab-on-a-printer technology. *Applied Sciences, 8*(12), 2414. doi:10.3390/app8122414

De Melo, B. A., Jodat, Y. A., Cruz, E. M., Benincasa, J. C., Shin, S. R., & Porcionatto, M. A. (2020). Strategies to use fibrinogen as bioink for 3D bioprinting fibrin-based soft and hard tissues. *Acta Biomaterialia, 117*, 60-76. doi:10.1016/j.actbio.2020.09.024

Dekel-Naftali, M., Aviram-Goldring, A., Litmanovitch, T., Shamash, J., Reznik-Wolf, H., Laevsky, I., Amit, M., Itskovitz-Eldor, J., Yung, Y., Hourvitz, A., Schiff, E., & Rienstein, S.. (2012). Screening of human pluripotent stem cells using CGH and FISH reveals low-grade mosaic aneuploidy and a recurrent amplification of chromosome 1q. *European Journal of Human Genetics, 20*(12), 1248–1255. doi.org/10.1038/ejhg.2012.128

Denton, K. R., Xu, C., Shah, H., & Li, X. J. (2016). Modeling Axonal Defects in Hereditary Spastic Paraplegia with Human Pluripotent Stem Cells. *Frontiers in biology, 11*(5), 339–354. doi.org/10.1007/s11515-016-1416-0

DeTure, M. A., & Dickson, D. W. (2019). The neuropathological diagnosis of lzheimer's disease. *Molecular Neurodegeneration, 14*(1). doi:10.1186/s13024-019-0333-5

Dimida, S., Barca, A., Cancelli, N., De Benedictis, V., Raucci, M. G., & Demitri, C. (2017). Effects of Genipin concentration on Cross-Linked Chitosan scaffolds for bone tissue Engineering: Structural characterization and evidence of Biocompatibility Features. *International Journal of Polymer Science,* 1-8. doi:10.1155/2017/8410750

Frew, J., Baradaran-Heravi, A., Balgi, A. D., Wu, X., Yan, T. D., Arns, S., Shidmoossavee, F. S., Tan, J., Jaquith, J. B., Jansen-West, K. R., Lynn, F. C., Gao, F., Petrucelli, L., Feldman, H. H., Mackenzie, I. R., Roberge, M., & Nygaard, H. B. (2020). Premature termination codon readthrough upregulates progranulin expression and improves lysosomal function in preclinical models of GRN deficiency. *Molecular Neurodegeneration, 15*(1), 21-21. doi.org/10.1186/s13024-020-00369-5

Galiakberova, A. A., & Dashinimaev, E. B. (2020). Neural stem cells and methods for their generation from induced pluripotent stem cells in vitro. Frontiers in Cell and *Developmental Biology, 8*, 815-815. doi.org/10.3389/fcell.2020.00815

Glenner, G. G. (2012). Reprint of "Alzheimer's disease: Initial report of the purification and characterization of a novel cerebrovascular amyloid protein". *Biochemical and Biophysical Research Communications, 425*(3), 534-539. doi:10.1016/j.bbrc.2012.08.020

Goedert, M., Spillantini, M. G., Jakes, R., Rutherford, D., & Crowther, R. A. (1989). Multiple isoforms of human microtubule-associated protein tau: Sequences and localization in neurofibrillary tangles of Alzheimer's disease. *Neuron, 3*(4), 519-526. doi:10.1016/0896-6273(89) 90210-9

Götz, J., Xia, D., Leinenga, G., Chew, Y. L., & Nicholas, H. (2013). What renders tau toxic. *Frontiers in Neurology, 4*(72). doi:10.3389/fneur.2013.00072

Grundke-Iqbal, I., Iqbal, K., Tung, Y. C., Quinlan, M., Wisniewski, H. M., & Binder, L. I. (1986). Abnormal phosphorylation of the microtubule-associated protein tau (tau) in alzheimer cytoskeletal pathology. *Proceedings of the National Academy of Sciences, 83*(13), 4913-4917. doi:10.1073/pnas.83.13.4913

Gunhanlar, N., Shpak, G., Van der Kroeg, M., Gouty-Colomer, L. A., Munshi, S. T., Lendemeijer, B., . . . Kushner, S. A. (2017). A simplified protocol for differentiation of electrophysiologically mature neuronal networks from human induced pluripotent stem cells. *Molecular Psychiatry, 23*(5), 1336-1344. doi:10.1038/mp.2017.56

Haase, A., Glienke, W., Engels, L., Göhring, G., Esser, R., Arseniev, L., & Martin, U. (2019). GMP-compatible manufacturing of three iPS cell lines from human peripheral blood. *Stem Cell Research, 35*. doi:10.1016/j.scr.2019.101394

Hanger, D. P., Byers, H. L., Wray, S., Leung, K., Saxton, M. J., Seereeram, A., Reynolds, C. H., Ward, M. A., & Anderton, B. H. (2007). Novel phosphorylation sites in tau from Alzheimer brain support a role for casein kinase 1 in disease pathogenesis. The Journal of Biological Chemistry, 282(32), 23645-23654. doi.org/10.1074/jbc.M703269200

Hernández-Sapiéns, M. A., Reza-Zaldívar, E. E., Cevallos, R. R., Márquez-Aguirre, A. L., Gazarian, K., & Canales-Aguirre, A. A. (2020). A three-dimensional Alzheimer's disease cell culture model using iPSC-derived neurons carrying A246E mutation in PSEN1. Frontiers in Cellular Neuroscience, 14, 151. doi.org/10.3389/fncel.2020.00151

Hippius, H., & Neundörfer, G. (2003). The discovery of Alzheimer's disease. *Dialogues in clinical neuroscience*, *5*(1), 101–108. doi.org/10.31887/DCNS.2003.5.1/hhippius

Holmes, O., Paturi, S., Ye, W., Wolfe, M. S., & Selkoe, D. J. (2012). Effects of membrane lipids on the activity and processivity of purified γ-secretase. *Biochemistry*, *51*(17), 3565–3575. doi.org/10.1021/bi300303g

Huang, Y., & Mahley, R. W. (2014). Apolipoprotein E: structure and function in lipid metabolism, neurobiology, and Alzheimer's diseases. *Neurobiology of disease*, *72*, 3–12. doi.org/10.1016/j.nbd.2014.08.025

Ittner, L. M., Fath, T., Ke, Y. D., Bi, M., Eersel, J. v., Li, K. M., Gunning, P., & Götz, J. (2008). Parkinsonism and impaired axonal transport in a mouse model of frontotemporal dementia. *Proceedings of the National Academy of Sciences, 105*(41), 15997-16002. doi.org/10.1073/pnas.0808084105

Jakel, S., & Dimou, L. (2017). Glial cells and their function in the adult brain: A journey through the history of their ablation. Frontiers in Cellular Neuroscience, 11, 24-24. doi.org/10.3389/fncel.2017.0002419/121.

Jensen, C., & Teng, Y. (2020). Is it time to start transitioning from 2D to 3D cell culture? *Frontiers in Molecular Biosciences, 7*. 33 doi:10.3389/fmolb.2020.00033

Kakuda, N., Funamoto, S., Yagishita, S., Takami, M., Osawa, S., Dohmae, N., & Ihara, Y. (2006). Equimolar production of Amyloid β-protein and amyloid precursor protein Intracellular domain from β-carboxyl-terminal Fragment by γ-Secretase. *Journal of Biological Chemistry, 281*(21), 14776-14786. doi:10.1074/jbc.m513453200

Kim, Y. S., Jung, H. M., & Yoon, B. E. (2018). Exploring glia to better understand Alzheimer's disease. *Animal cells and systems, 22*(4), 213–218. doi.org/10.1080/19768354.2018.1508498

Kimura, T., Sharma, G., Ishiguro, K., & Hisanaga, S. (2018). Phospho-Tau bar Code: Analysis of phosphoisotypes of tau and its application to Tauopathy. *Frontiers in Neuroscience, 12*. doi:10.3389/fnins.2018.00044

Kjar, A., McFarland, B., Mecham, K., Harward, N., & Huang, Y. (2021). Engineering of tissue constructs using coaxial bioprinting. *Bioactive Materials, 6*(2), 460-471. doi:10.1016/j.bioactmat.2020.08.020

Kojro, E., & Fahrenholz, F. (2005). The non-amyloidogenic pathway: Structure and function of α-secretases. *Subcellular Biochemistry, 38*, 105-127. doi:10.1007/0-387-23226-5_5

Köpke, E., Tung, Y. C., Shaikh, S., Alonso, A. C., Iqbal, K., & Grundke-Iqbal, I. (1993). Microtubule-associated protein tau. Abnormal phosphorylation of a non-paired helical filament pool in Alzheimer disease. *The Journal of biological chemistry*, *268*(32), 24374–24384.

Labour, M., Vigier, S., Lerner, D., Marcilhac, A., & Belamie, E. (2016). 3D compartmented model to study the neurite-related toxicity of Aβ aggregates included in collagen gels of adaptable porosity. *Acta Biomaterialia, 37*, 38-49. doi.org/10.1016/j.actbio.2016.04.001

Lee, C., Willerth, S. M., & Nygaard, H. B. (2020). The use of patient-derived induced pluripotent stem cells for Alzheimer's disease modeling. *Progress in Neurobiology, 192*, 101804. doi.org/10.1016/j.pneurobio.2020.101804

Lee, K. Y., & Mooney, D. J. (2012). Alginate: properties and biomedical applications. *Progress in polymer science*, *37*(1), 106–126. doi.org/10.1016/j.progpolymsci.2011.06.003

Lin, WL., Lewis, J., Yen, SH., Hutton, M., & Dennis, D. (2003). Ultrastructural neuronal pathology in transgenic mice expressing mutant (P301L) human tau. *Journal of Neurocytology 32*, 1091–1105 . doi.org/10.1023/B:NEUR.0000021904.61387.9

Lindsay, J. (2002). Risk factors for Alzheimer's disease: A Prospective analysis from the Canadian study of health and aging. *American Journal of Epidemiology, 156*(5), 445-453. doi:10.1093/aje/kwf074

Liu, C., Kanekiyo, T., Xu, H., & Bu, G. (2013). Apolipoprotein E and Alzheimer disease: Risk, mechanisms and therapy. *Nature Reviews Neurology, 9*(2), 106-118. doi:10.1038/nrneurol.2012.263

Mangialasche, F., Solomon, A., Winblad, B., Mecocci, P., & Kivipelto, M. (2010). Alzheimer's disease: Clinical trials and drug development. *The Lancet Neurology, 9*(7), 702-716. doi:10.1016/s1474-4422(10)70119-8

Maqbool, M., Mobashir, M., & Hoda, N. (2016). Pivotal role of glycogen synthase kinase-3: A therapeutic target for Alzheimer's disease. *European Journal of Medicinal Chemistry, 107*, 63-81. doi:10.1016/j.ejmech.2015.10.018

Mariani, J., Simonini, M. V., Palejev, D., Tomasini, L., Coppola, G., Szekely, A. M., Horvath, T. L., & Vaccarino, F. M. (2012). Modeling human cortical development in vitro using induced pluripotent stem cells. *Proceedings of the National Academy of Sciences, 109*(31), 12770-12775. doi.org/10.1073/pnas.1202944109

Martínez-Cerdeño, V., & Noctor, S. C. (2018). Neural progenitor cell terminology. *Frontiers in Neuroanatomy, 12*. doi:10.3389/fnana.2018.00104

McKhann, G., Drachman, D., Folstein, M., Katzman, R., Price, D., & Stadlan, E. M. (2011). Clinical diagnosis of Alzheimer's disease: Report of The NINCDS--ADRDA work group under the auspices of Department of health and Human Services Task force on Alzheimer's disease. *Neurology, 77*(4), 939. doi:10.1212/01.wnl.0000400650.92875.cf

Medline Plus. (2020, August 18). PSEN1 gene: MedlinePlus Genetics. Retrieved March 13, 2021, from https://medlineplus.gov/genetics/gene/psen1/#conditions

Meyer, G., Perez-Garcia, C. G., Abraham, H., & Caput, D. (2002). Expression of p73 and reelin in the developing human cortex. *The Journal of Neuroscience, 22*(12), 4973-4986. doi:10.1523/jneurosci.22-12-04973.2002

Mockett, B. G., Richter, M., Abraham, W. C., & Müller, U. C. (2017). Therapeutic potential of secreted amyloid precursor protein appsα. *Frontiers in Molecular Neuroscience, 10*. doi:10.3389/fnmol.2017.00030

Neural tube. (2014). Retrieved March 13, 2021, from https://www.sciencedirect.com/topics/neuroscience/neural-tube#:~:text=The%20neural%20tube%20is%20the,its%20formation%20is%20called%20neurulation

Neve, R. L., Harris, P., Kosik, K. S., Kurnit, D. M., & Donlon, T. A. (1986). Identification of cDNA clones for the human microtubule-associated protein tau and chromosomal localization of the genes for tau and microtubule-associated protein 2. *Molecular Brain Research, 1*(3), 271-280. doi:10.1016/0169-328x(86)90033-1

Nicolas, J., Magli, S., Rabbachin, L., Sampaolesi, S., Nicotra, F., & Russo, L. (2020). 3D extracellular Matrix Mimics: Fundamental concepts and role of materials chemistry to influence stem Cell Fate. *Biomacromolecules, 21*(6), 1968-1994. doi:10.1021/acs.biomac.0c00045

O'Brien, R. J., & Wong, P. C. (2011). Amyloid precursor protein processing and Alzheimer's disease. *Annual Review of Neuroscience, 34*(1), 185-204. doi:10.1146/annurev-neuro-061010-113613

Ozbolat, I. T., & Hospodiuk, M. (2016). Current advances and future perspectives in extrusion-based bioprinting. *Biomaterials, 76*, 321-343. doi:10.1016/j.biomaterials.2015.10.076

Papadimitriou, C., Celikkaya, H., Cosacak, M. I., Mashkaryan, V., Bray, L., Bhattarai, P., Brandt, K., Hollak, H., Chen, X., He, S., Antos, C. L., Lin, W., Thomas, A. K., Dahl, A., Kurth, T., Friedrichs, J., Zhang, Y., Freudenberg, U., Werner, C., & Kizil, C. (2018). 3D culture method for Alzheimer's disease modeling reveals interleukin-4 rescues Aβ42-induced loss of human neural stem cell plasticity. *Developmental Cell, 46*(1), 85-101. doi.org/10.1016/j.devcel.2018.06.005

Pchitskaya, E., & Bezprozvanny, I. (2020). Dendritic spines shape analysis-classification or clusterization? perspective. *Frontiers in Synaptic Neuroscience, 12*, 31-31. doi.org/10.3389/fnsyn.2020.00031

Perlman R. L. (2016). Mouse models of human disease: An evolutionary perspective. *Evolution, medicine, and public health*, *2016*(1), 170–176. doi.org/10.1093/emph/eow014

Piaceri, I., Nacmias, B., & Sorbi, S. (2013). Genetics of familial and sporadic Alzheimer's disease. *Frontiers in bioscience*, *5*, 167–177. doi.org/10.2741/e605

Prince, M., Anders, W., Guerchet, M., Ali, G., Wu, Y., & Prina, M. (2016). World Alzheimer Report 2015: The global impact of dementia: An analysis of prevalence, incidence, cost and trends. *Alzheimer's & Dementia, 8*(23). doi:10.1016/j.jalz.2015.06.185

Qiu, T. (2015). Aβ42 and Aβ40: Similarities and differences. *Journal of Peptide Science, 21*(7), 522-529. doi.org/10.1002/psc.2789

Rabinovici G. D. (2019). Late-onset Alzheimer Disease. *Continuum*, *25*(1), 14–33. doi.org/10.1212/CON.0000000000000700

Reynolds, C. H., Nebreda, A. R., Gibb, G. M., Utton, M. A., & Anderton, B. H. (2002). Reactivating kinase/p38 phosphorylates τ protein in vitro. *Journal of Neurochemistry, 69*(1), 191-198. doi:10.1046/j.1471-4159.1997.69010191.x

Robinson, M., Douglas, S., & Michelle Willerth, S. (2017). Mechanically stable fibrin scaffolds promote viability and induce neurite outgrowth in neural aggregates derived from human induced pluripotent stem cells. *Scientific Reports, 7*(1). doi:10.1038/s41598-017-06570-9

Rose S. E, Frankowski H, Knupp A, Berry B. J, Martinez R, Dinh S. Q, Bruner L. T,Willis S. L, Crane P. K, Larson E. B, et al. Leptomeninges-derived induced pluripotent stem cells and directly converted neurons from autopsy caseswith varying Neuropathologic backgrounds. *Journal Neuropathology and Experimental Neurology.77*, 353–60

Sakono, M., & Zako, T. (2010). Amyloid oligomers: Formation and toxicity of Aβ oligomers. *FEBS Journal, 277*(6), 1348-1358. doi:10.1111/j.1742-4658.2010.07568.x

Salaris, Colosi, Brighi, Soloperto, Turris, Benedetti, Ghirga, Rosito, Angelantonio, D., & Rosa. (2019). 3D bioprinted human cortical neural constructs derived from induced pluripotent stem cells. *Journal of Clinical Medicine, 8*(10), 1595. doi.org/10.3390/jcm8101595

Schek, R. M., Michalek, A. J., & Iatridis, J. C. (2011). Genipin-crosslinked fibrin hydrogels as a potential adhesive to augment intervertebral disc annulus repair. *European cells & materials*, *21*, 373–383. doi.org/10.22203/ecm.v021a28

Science Direct. (n.d.). Anoikis. Retrieved March 13, 2021, from https://www.sciencedirect.com/topics/medicine-and-dentistry/anoikis

Shen, J., & Kelleher, R. J. (2006). The presenilin hypothesis of Alzheimer's disease: Evidence for a loss-of-function pathogenic mechanism. *Proceedings of the National Academy of Sciences, 104*(2), 403-409. doi:10.1073/pnas.0608332104

Sherriff, F. E., Bridges, L. R., Gentleman, S. M., Sivaloganathan, S., & Wilson, S. (1994). Markers of axonal injury in postmortem human brain. *Acta Neuropathologica, 88*(5), 433-439. doi.org/10.1007/s004010050181

Sinha, S., Anderson, J. P., Tan, H., Power, M., Jewett, N., Seubert, P., Davis, D., McConlogue, L., Frigon, N., Schenk, D., Barbour, R., Tung, J., Suomensaari, S. M., Zhao, J., Basi, G. S., Knops, J., Wang, S., Walker, D., Hong, J., . . . Caccavello, R. (1999). Purification and cloning of amyloid precursor protein β-secretase from human brain. Nature (London), 402(6761), 537-540. doi.org/10.1038/990114

Soriano, S., Chyung, A. S., Chen, X., Stokin, G. B., Lee, V. M., & Koo, E. H. (1999). Expression of ß-amyloid precursor Protein-cd3γ chimeras to demonstrate the selective generation of Amyloid ß1–40 and Amyloid β1–42 Peptides within secretory and endocytic compartments. *Journal of Biological Chemistry, 274*(45), 32295-32300. doi:10.1074/jbc.274.45.32295

Stokin, G. B., Lillo, C., Falzone, T. L., Brusch, R. G., Rockenstein, E., Mount, S. L., Raman, R., Davies, P., Masliah, E., Williams, D. S., & Lawrence S. B. Goldstein. (2005). Axonopathy and transport deficits early in the pathogenesis of Alzheimer's disease. *Science, 307*(5713), 1282-1288. doi.org/10.1126/science.1105681

Sugitani, Y., Nakai, S., Minowa, O., Nishi, M., Jishage, K., Kawano, H., Mori, K., Ogawa, M., & Noda, T. (2002). Brn-1 and brn-2 share crucial roles in the production and positioning of mouse neocortical neurons. *Genes & Development, 16*(14), 1760-1765. https://doi.org/10.1101/gad.978002

Takahashi, K., & Yamanaka, S. (2006). Induction of Pluripotent Stem Cells from Mouse Embryonic and Adult Fibroblast Cultures by Defined Factors. *Cell, 126*(4), 663-676. doi.org/10.1016/j.cell.2006.07.024

Takahashi, K., Tanabe, K., Ohnuki, M., Narita, M., Ichisaka, T., Tomodo, K., & Yamanaka, S. (2007). Induction of Pluripotent Stem Cells from Adult Human Fibroblasts by Defined Factors. *Cell, 131*(5), 861-872. doi.org/10.1016/j.cell.2007.11.019

Tcw, J., & Goate, A. M. (2017). Genetics of β-Amyloid Precursor Protein in Alzheimer's Disease. *Cold Spring Harbor perspectives in medicine*, *7*(6). doi.org/10.1101/cshperspect.a024539

Thomas, M., & Willerth, S. M. (2017). 3-D Bioprinting of neural tissue for applications in cell therapy and drug screening. *Frontiers in Bioengineering and Biotechnology, 5*(69). doi:10.3389/fbioe.2017.00069

Toh, W. H., Tan, J. Z., Zulkefli, K. L., Houghton, F. J., & Gleeson, P. A. (2017). Amyloid precursor protein traffics from the Golgi directly to early endosomes in an ARL5B- and AP4-dependent pathway. *Traffic, 18*(3), 159-175. doi:10.1111/tra.12465

United Nations. (n.d.). World population prospects 2019. Retrieved March 13, 2021, from https://population.un.org/wpp/Publications/Files/WPP2019_Volume-I_Comprehensive-Tables.pdf

Vassar, R. (2003). Bace1: The β-secretase enzyme in alzheimer's disease. *Journal of Molecular Neuroscience, 23*(12), 105-114. doi:10.1385/jmn:23:1-2:105

Walker, E. S., Martinez, M., Brunkan, A. L., & Goate, A. (2005). Presenilin 2 familial Alzheimer's disease mutations result in partial loss of function and dramatic changes in abeta 42/40 ratios. *Journal of Neurochemistry, 92*(2), 294-301. doi:10.1111/j.1471-4159.2004.02858.x

Walsh, D. M., Minogue, A. M., Sala Frigerio, C., Fadeeva, J. V., Wasco, W., & Selkoe, D. J. (2007). The APP family of proteins: similarities and differences. *Biochemical Society transactions*, *35*, 416–420. doi.org/10.1042/BST0350416

Weingarten, M., Lockwood, A., Hwo, S., & Kirschner, M. (1975). A Protein Factor Essential for Microtubule Assembly. *Proceedings of the National Academy of Sciences of the United States of America, 72*(5), 1858-1862. doi.org/10.1073/pnas.72.5.1858

Weisel, J. W., & Litvinov, R. I. (2013). Mechanisms of fibrin polymerization and clinical implications. *Blood*, *121*(10), 1712–1719. doi.org/10.1182/blood-2012-09-306639

Wilson, P. G., & Stice, S. S. (2006). Development and differentiation of neural rosettes derived from human embryonic stem cells. *Stem Cell Reviews, 2*(1), 67-77. doi:10.1007/s12015-006-0011-1

Wisniewski, K. E., Wisniewski, H. M., & Wen, G. Y. (1985). Occurrence of neuropathological changes and dementia of Alzheimer's disease in Down's syndrome. *Annals of Neurology, 17*(3), 278-282. doi:10.1002/ana.410170310

Zhang, D., Pekkanen-Mattila, M., Shahsavani, M., Falk, A., Teixeira, A. I., & Herland, A. (2014). A 3D alzheimer's disease culture model and the induction of p21-activated kinase mediated sensing in iPSC derived neurons. *Biomaterials, 35*(5), 1420-1428. doi:10.1016/j.biomaterials.2013.11.028

Zhang, H., Ma, Q., Zhang, Y., & Xu, H. (2011). Proteolytic processing of Alzheimer's ß-amyloid precursor protein. *Journal of Neurochemistry, 120*, 9-21. doi:10.1111/j.1471-4159.2011.07519.x

Zhang, M., Ngo, J., Pirozzi, F., Sun, Y., & Wynshaw-Boris, A. (2018). Highly efficient methods to obtain homogeneous dorsal neural progenitor cells from human and mouse embryonic stem cells and induced pluripotent stem cells. *Stem Cell Research & Therapy, 9*(1), 67-67. doi.org/10.1186/s13287-018-0812-6

Zhang, X., & Song, W. (2013). The role of app and BACE1 trafficking in app processing and amyloid-β generation. *Alzheimer's Research & Therapy, 5*(46). doi:10.1186/alzrt211

Zheng, W., Li, Q., Zhao, C., Da, Y., Zhang, H., & Chen, Z. (2018). Differentiation of glial cells from hiPSCs: Potential applications in neurological diseases and cell replacement therapy. *Frontiers in Cellular Neuroscience, 12*, 239-239. https://doi.org/10.3389/fncel.2018.00239